Article:

Hutchison, W, Mather, TA, Pyle, DM et al. (9 more authors) (2018) The evolution of magma during continental rifting: New constraints from the isotopic and trace element signatures of silicic magmas from Ethiopian volcanoes. Earth and Planetary Science Letters, 489. pp. 203-218. ISSN 0012-821X

https://doi.org/10.1016/j.epsl.2018.02.027

The evolution of magma during continental rifting: new constraints from the isotopic and trace element signatures of silicic magmas from Ethiopian volcanoes

William Hutchison[1, 2], Tamsin A. Mather[1], David M. Pyle[1], Adrian J. Boyce[3], Matthew L. M. Gleeson[4], Gezahegn Yirgu[5], Jon D. Blundy[6], David J. Ferguson[7], Charlotte Vye-Brown[8], Ian L. Millar[9], Kenneth W.W. Sims[10] and Adrian A. Finch[2]

[1] Department of Earth Sciences, University of Oxford, South Parks Road, Oxford OX1 3AN, UK. [2] School of Earth and Environmental Sciences, University of St. Andrews, KY16 9AL, UK. [3] Scottish Universities Environmental Research Centre, Rankine Avenue, East Kilbride G75 0QF, UK. [4] Department of Earth Sciences, University of Cambridge, Downing Street, Cambridge CB2 3EQ, UK. [5] School of Earth Sciences, Addis Ababa University, P.O. Box 1176, Addis Ababa, Ethiopia. [6] School of Earth Sciences, University of Bristol, Wills Memorial Building, Queens Road, Bristol BS8 1RJ, UK. [7] School of Earth and Environment, University of Leeds, Leeds LS2 9JT, UK. [8] British Geological Survey, The Lyell Centre, Research Avenue South, Edinburgh EH14 4AP, UK. [9] NERC Isotope Geosciences Laboratory, Keyworth, Nottingham, NG12 5GG, UK. [10] Department of Geology and Geophysics, University of Wyoming, Laramie, WY 82071, USA.

Corresponding author: William Hutchison (wh39@st-andrews.ac.uk)

Highlights:

- First ‘rift-scale’ analysis of silicic magmagenesis in Ethiopia
- Limited assimilation of high-$\delta^{18}O$ Pan-African basement in Quaternary magmas

- Fractional crystallization is variable and amplified in regions of low magma flux
- We predict ~45 Ma of magmatic intrusion has removed fusible components from crust
- Greater crustal assimilation for Oligocene magmas supports secular variations

Keywords: rift; magmatism; assimilation; peralkaline; Ethiopia; oxygen isotopes

Abstract

Magma plays a vital role in the break-up of continental lithosphere. However, significant uncertainty remains about how magma-crust interactions and melt evolution vary during the development of a rift system. Ethiopia captures the transition from continental rifting to incipient sea-floor spreading and has witnessed the eruption of large volumes of silicic volcanic rocks across the region over ~45 Ma. The petrogenesis of these silicic rocks sheds light on the role of magmatism in rift development, by providing information on crustal interactions, melt fluxes and magmatic differentiation. We report new trace element and Sr-Nd-O isotopic data for volcanic rocks, glasses and minerals along and across active segments of the Main Ethiopian (MER) and Afar Rifts. Most $\delta^{18}O$ data for mineral and glass separates from these active rift zones fall within the bounds of modelled fractional crystallization trajectories from basaltic parent magmas (i.e., 5.5–6.5 ‰) with scant evidence for assimilation of Pan-African Precambrian crustal material ($\delta^{18}O$ of 7–18 ‰). Radiogenic isotopes (ε_{Nd}=0.92–6.52; $^{87}Sr/^{86}Sr$ = 0.7037–0.7072) and incompatible trace element ratios (Rb/Nb <1.5) are consistent with $\delta^{18}O$ data and emphasize limited interaction with Pan-African crust. However, there are important regional variations in melt evolution revealed by incompatible elements (e.g., Th and Zr) and peralkalinity (molar

Na_2O+K_2O/Al_2O_3). The most chemically-evolved peralkaline compositions are associated with the MER volcanoes (Aluto, Gedemsa and Kone) and an off-axis volcano of the Afar Rift (Badi). On-axis silicic volcanoes of the Afar Rift (e.g., Dabbahu) generate less-evolved melts. While at Erta Ale, the most mature rift setting, peralkaline magmas are rare. We find that melt evolution is enhanced in less mature continental rifts (where parental magmas are of transitional rather than tholeiitic composition) and regions of low magma flux (due to reduced mantle melt productivity or where crustal structure inhibits magma ascent). This has important implications for understanding the geotectonic settings that promote extreme melt evolution and, potentially, genesis of economically-valuable mineral deposits in ancient rift-settings. The limited isotopic evidence for assimilation of Pan-African crustal material in Ethiopia suggests that the pre-rift crust beneath the magmatic segments has been substantially modified by rift-related magmatism over the past ~45 Ma; consistent with geophysical observations. We argue that considerable volumes of crystal cumulate are stored beneath silicic volcanic systems (> 100 km^3), and estimate that crystal cumulates fill at least 16–30 % of the volume generated by crustal extension under the axial volcanoes of the MER and Manda Hararo Rift Segment (MHRS) of Afar. At Erta Ale only ~1 % of the volume generated due to rift extension is filled by cumulates, supporting previous seismic evidence for a greater role of plate stretching in mature rifts at the onset of sea-floor spreading. We infer that ~45 Ma of magmatism has left little fusible Pan-African material to be assimilated beneath the magmatic segments and the active segments are predominantly composed of magmatic cumulates with $\delta^{18}O$ indistinguishable from mantle-derived melts. We predict that the $\delta^{18}O$ of silicic magmas should converge to mantle values as the rift continues to evolve. Although current data are limited, a comparison with ~30 Ma ignimbrites (with $\delta^{18}O$ up

to 8.9 ‰) supports this inference, evidencing greater crustal assimilation during initial stages of rifting and at times of heightened magmatic flux.

1. Introduction

Magmatism fundamentally alters the thermal, chemical and mechanical properties of the crust and plays a key role in the break-up of continental lithosphere (Buck, 2006; Bialas et al., 2010). However, uncertainty remains about whether magmatic differentiation and crustal interactions vary spatially between different rift segments, and whether there are significant secular variations during rift evolution. Studies of the petrogenesis of rift magmas offer insights into these questions.

The petrologic diversity of volcanic rocks is generated by numerous processes. Among the most important are: interaction with the crust via partial melting or assimilation; and fractional crystallization of the parental magma (e.g., Macdonald et al., 2008; Deering et al., 2008). Partial crustal melting strongly depends on the thermal state of the crust (Dufek and Bergantz, 2005; Annen et al., 2006) and the availability of fusible crustal materials. In active rifts, the potential for partial melting will be amplified in regions of elevated temperatures and will coincide with zones of highest magmatic intrusion (Karakas and Dufek, 2015). Partial melting is also favoured in regions of fusible crust, while more refractory regions, that have already been heavily intruded, are less likely to be remelted or assimilated by later intrusions. Fractional crystallization will be amplified in rift settings where magma flux and crustal temperatures are lower, and there is an absence of fusible crust.

Geochemical techniques can discriminate between partial crustal melting and fractional crystallization. Oxygen isotopes ($\delta^{18}O$) are a powerful tool for investigating crustal interactions (provided the $\delta^{18}O$ of crust is distinct from mantle-derived rocks and cumulates), while incompatible trace elements (e.g., Ba, Sr, Th, Zr) are particularly sensitive to fractional crystallization. Geochemical studies in active rift zones, notably Iceland, have successfully linked silicic magma petrogenesis to the thermal state of the crust (Martin and Sigmarsson, 2010). On the axis of the Icelandic Rift, where magma flux is high and the crust is hot, silicic magmas exhibit $\delta^{18}O$ evidence for assimilation of fusible hydrothermally-altered metabasaltic crust with low $\delta^{18}O$ (< 2 ‰). While in cooler off-rift settings, magmatic flux is lower, assimilation is limited (samples exhibit normal magmatic $\delta^{18}O$, 5.0–6.5‰, Eiler, 2001), and silicic melts undergo extensive fractional crystallization. In continental rift zones further complexity is expected because vestigial pre-rift continental crust may also be present.

Ethiopia exposes several stages of rift development from continental rifting in the Main Ethiopian Rift (MER) to nascent seafloor spreading in the Afar Rift (Figure 1, Hayward and Ebinger, 1996), providing a unique opportunity to study connections between magma petrogenesis and geotectonic setting. Here, geochemical data can be interpreted in the context of geophysical constraints on crustal structure and composition (Keranen et al., 2004; Bastow and Keir, 2011; Hammond et al., 2011), and magmatic intrusion volumes (Dessisa et al., 2013; Keir et al., 2015). Further, magmatism in Ethiopia has been taking place since ~45 Ma (Rooney, 2017) permitting the development of a temporal understanding of magma evolution and crustal interactions as rifting proceeds.

Previous studies in Ethiopia focused on geochemistry of mafic magmas of the MER and found evidence for spatio-temporal variations in crustal assimilation and fractionation (Rooney et al., 2007; Section 2). However, silicic volcanism is a key component of rift magmatism and a common feature across different rift zones. Although previous authors have investigated individual complexes (e.g., Gedemsa, Peccerillo et al., 2003; Dabbahu, Field et al., 2013) it is unclear whether silicic magmagenesis varies spatially across different rift settings and whether there have been secular variations since the onset of rifting. Answering these questions has important implications for understanding ongoing rift volcanism; and the links between petrogenesis, rift setting and mineral resources. Silicic melts generated in continental rifts by protracted fractional crystallization tend to be enriched in economically-valuable elements (including, rare earth elements, REE, Zr, Nb and Ta). Identifying rift settings that favour extreme differentiation (i.e., mature versus immature continental rifts, or on- versus off-axis locations) provides valuable insights into the geotectonic settings that may host economically significant ore bodies.

In this paper we integrate new and published Sr-Nd-O isotope and trace element data from six MER and Afar Rift volcanic systems (Figure 1a, b). We evaluate the relative importance of fractional crystallization and crustal melting at each and compare this to their rift setting (crustal thickness and crustal compositions, Figure 1) and eruptive flux. We show that:

- **i)** despite significant variations in magma flux and crustal structure there is limited evidence for Pan-African crustal assimilation in Ethiopian Quaternary magmas
- **ii)** there are variations in fractional crystallization between the different volcanic systems, and melt evolution is amplified in less mature rifts with lower magma flux
- **iii)** the relative importance of fractional crystallization and crustal melting in the genesis of silicic magmas should vary as a continental rift develops and the pre-rift crust is modified by magmatic intrusions

2. Geological Setting

Magmatic activity in East Africa began in the Eocene. Recent reviews (Rooney, 2017) suggest multiple pulses of magmatism since ~45 Ma, with the most volumetrically-significant flood basalt and silicic eruptions taking place in the Oligocene (~33.9 to 27 Ma, Hofmann et al., 1997; Ayalew et al., 2002). Rift magmas have intruded through a continental lithosphere that comprises Precambrian schists and granitoids assembled during the Neoproterozoic Pan-African crust building event (Teklay et al., 1998). Initiation of major rift zones was diachronous: ~35 Ma in the Gulf of Aden (d'Acremont et al., 2005); ~28 Ma in the Red Sea (Wolfenden et al., 2005) and 15–18 Ma in the MER (Wolfenden et al., 2004). Each rift zone shows a comparable evolutionary history, with early deformation accommodated on border faults, and later extension and magmatic intrusions localized along 20 km wide and 60–80 km long magmatic segments (Ebinger, 2005). Geological and geophysical evidence for crustal thinning (Maguire et al., 2006; Hammond et al., 2011, Bastow and Keir, 2011), intruded magma volumes (Keranen et al., 2004; Keir et al., 2015) and rift architecture (Agostini et al., 2011) suggest rift maturity varies from intermediate-mature continental rifting in the MER to incipient seafloor spreading in Afar.

Quaternary volcanism in Ethiopia is strongly bimodal; basalts (mantle melts generated at significant depths, >80 km, and elevated temperatures, Rooney et al., 2012a; Ferguson et al., 2013a; Armitage et al., 2015) are associated with dykes and fissure eruptions, whereas rhyolites and trachytes are associated with shield-like complexes and calderas.

We focus on six volcanic systems (Figure 1a). Aluto, Gedemsa and Kone are located along the MER (Kone is in a different magmatic segment from Aluto and Gedemsa; Ebinger and Casey, 2001). In the Afar Rift, Dabbahu and Badi are located on and off the Manda Hararo Rift Segment (MHRS), respectively (Figure 1b), while the northerly Erta Ale range comprises the

Erta Ale Segment (EAS, Beyene and Abdelsalam, 2005). Table 1 summarizes the setting and eruptive history of the volcanic systems. Based on published data, each volcanic system spans a wide compositional range (45–75 wt. % SiO_2), and is represented predominantly by basalt and rhyolite compositions (Figure 2a). Although rocks with intermediate silica contents are relatively scarce there is a continuum of compositions (c.f. Macdonald et al., 2008) and only Kone (Figure 1a) completely lacks intermediate magmas (Figure 2a). Basalts from Erta Ale are notably more tholeiitic than the other complexes, and maintain lower alkalinity throughout the differentiation sequence.

Crustal thickness varies markedly between different rift zones, from ~16 km in the EAS to 20–22 km beneath the MHRS, and from ~40 km in the MER beneath Aluto to ~30 km beneath Kone (Maguire et al., 2006, Figure 1c). The upper crust comprises vestigial Pan-African crust (Figure 1c, Makris and Ginzburg 1987; Mackenzie et al., 2005; Maguire et al., 2006; Hammond et al., 2011) with $\delta^{18}O$ of 7–18 ‰ (Duffield et al., 1997; Ayalew et al., 2002), higher than typical mantle-derived magmas (5–6.5‰, Section 5.1). Geophysical surveys suggest that the Pan-African crust has been significantly modified by intrusions (particularly beneath magmatic segments, Hammond et al., 2011). This is supported by geochemical studies of mafic lavas which show, firstly, that crustal assimilation in Quaternary lavas is only identified in less mature, more southerly, MER rift sections; secondly, that crustal assimilation is more pronounced in older lava series (30 and 11–6 Ma) compared to recent samples (Rooney et al., 2007). Silicic magmas, the topic of this study, have a longer residence in the crust and provide a complementary and potentially more accentuated geochemical record of magma-crust interaction and fractionation.

3. Methods

3.1 Analytical methods

$\delta^{18}O$ analysis of glass and mineral separates (1–2 mg) was carried out at Scottish Universities Environmental Research Centre, East Kilbride by laser fluorination following the method of Sharp (1990) modified for ClF_3 (Macaulay et al., 2000). For mineral separates, overnight prefluorination was carried out to remove adsorbed environmental water from the sample chamber and line. For glasses, which are more reactive in ClF_3, we employed a short (90 second) room-temperature prefluorination before each analysis (Pope et al., 2013). Standards were run after each unknown and their reproducibility errors, including mass spectrometry, was typically better than ±0.3 ‰, reported in standard notation as permil (‰) variations to V-SMOW. New analyses are compiled in Table 2. To complement the $\delta^{18}O$, a small number of samples were analysed for Sr-Nd-Pb isotopes. Detailed information on the preparation and analysis of these samples is provided in the Supplementary Information with a compilation of all whole-rock major and trace element data used here (Supplementary Data).

3.2 Thermodynamic and oxygen isotope modelling

To examine whether evolved peralkaline magmas could be generated via closed-system fractional crystallization only, we modelled potential differentiation sequences using Rhyolite-MELTS (Gualda et al., 2012). Using a primitive parental basalt composition (Table 3) and assuming isobaric fractional crystallization, we calculated the stable phase assemblage, at given pressure (P), temperature (T) and oxygen fugacity (fO_2), most closely matching the composition of natural samples. We focused modelling on Aluto and Dabbahu as their sample suites have been analysed in greatest detail (Field et al., 2013; Gleeson et al., 2017). A range of parameters was explored (Table 3), and a minimization routine used to identify the best-fit P, T and fO_2 conditions matching whole-rock data (Gleeson et al., 2017). While there are well-known limitations applying Rhyolite-MELTS to peralkaline systems (discussed by Rooney et al., 2012b; Gleeson et al., 2017), models provide a reasonable fit to the compositional data and are sufficient to gain first-order understanding of the liquid lines of descent and crystallization sequence required to generate silicic peralkaline melts.

Few studies have investigated the variation of $\delta^{18}O$ in peralkaline magma. We model the expected changes in $\delta^{18}O_{melt}$ during closed-system fractional crystallization using the approach of Bindeman et al. (2004). Taking the step-wise crystallizing assemblage, temperature and melt composition from the best-fitting Rhyolite-MELTS model, we calculate $\delta^{18}O_{cumulate}$ and subtract this from the $\delta^{18}O_{melt}$ value. We treated the melt as a mixture of CIPW normative minerals, and calculate the temperature and melt composition-dependent mineral-melt fractionations ($\Delta_n^{i+1}(T)$) at each step (i+1) and for each crystallizing mineral (n). This forward-step mass balance model (detailed in the Supplementary Information) follows equations from Bucholz et al. (2017). We determine $\delta^{18}O_{melt}$ at each stage of peralkaline melt genesis from primitive rift-related basalts and predict the $\delta^{18}O$ trajectory that may plausibly represent the products of closed-system fractional crystallization. Samples that fall off the modelled $\delta^{18}O_{melt}$ fractionation trajectory have likely assimilated local crust (see Section 5.1).

4. Results

4.1 Major element trends and Rhyolite-MELTS models

Silicic rocks from Ethiopia are mainly peralkaline (i.e., molar Na_2O + K_2O / Al_2O_3, NK/A, >1; Figure 2b). The most peralkaline samples (NK/A >1.6) are associated with the MHRS off-axis volcano Badi and MER volcanoes Kone, Gedemsa and Aluto. Erta Ale samples are only mildly peralkaline, while peraluminous rocks (i.e., molar Al_2O_3 / CaO + K_2O + Na_2O >1) are found at Gedemsa (Figure 2b). The volcanic systems are more clearly distinguished using the peralkaline classification diagram of Macdonald et al. (1974) that shows all complexes, except Erta Ale, are dominated by pantellerites, with lesser comendites (Figure 2c). Kone, Gedemsa, Aluto and Badi erupt the most evolved pantelleritic melts (Figure 2c).

Major element trends overlap (Figure 3), suggesting a similar pattern of crystallization and melt evolution at each system. The most obvious major element differences are observed in samples with >70 wt. % SiO_2. Rhyolites show considerable scatter in FeO_t values, reflecting varying degrees of fayalite, alkali pyroxene, aenigmatite and Fe-Ti oxide removal or accumulation in the final stages of melt evolution. Rhyolites with anomalously low Na_2O (Gedemsa and Kone samples, Figure 3) tend to have high loss on ignition, perhaps reflecting post-emplacement alteration (Peccerillo et al., 2003). There is considerable scatter in Al_2O_3 above 70 wt. % SiO_2 suggesting that feldspar fractionation is highly variable, while the Al_2O_3 minima suggest that more extensive feldspar fractionation occurred at Kone, Gedemsa, Aluto and Badi compared to Dabbahu and Erta Ale (Figure 3). P_2O_5 for most suites falls on a non-linear trend with an inflection at ~55 wt. % SiO_2 that reflects stabilization of apatite (Rooney et al., 2012b; Field et al., 2013). The behaviour of P_2O_5 suggests that fractional crystallization is the main process generating the magmas (c.f. Lee and Bachmann, 2014), although a few enclaves from Gedemsa

(Peccerillo et al., 2003) and basaltic trachyandesites from Dabbahu (Field et al., 2011) fall along trends consistent with magma-mixing (Figure 3).

Rhyolite-MELTS fractional crystallization models for Aluto and Dabbahu reproduce reasonably well the trends observed in whole-rock data (Figure 3). In both cases the best-fit models were able to generate pantellerite melts from the most primitive mafic samples at low pressures (150 MPa), low initial H_2O concentrations (~0.5 wt. %) and relatively low fO_2 (QFM; Table 3). Rhyolite-MELTS modelling is consistent with pantellerites being produced by protracted fractional crystallization (>80 %) of primitive rift-related basalts (Gleeson et al., 2017). Discrepancies between Rhyolite-MELTS models and whole-rock data are generally restricted to the final stages of crystallization (>65 wt. % SiO_2), as explored by Rooney et al. (2012) and Gleeson et al. (2017). In short, the Rhyolite-MELTS apatite solubility model overpredicts P_2O_5 for peralkaline magmas throughout fractionation (Rooney et al., 2012b). CaO is also overpredicted, linked to inaccuracies in the stabilization of apatite (Rooney et al., 2012b). FeO_t concentrations for Rhyolite-MELTS models are 1–6 wt. % lower than natural sample values at high SiO_2 (>65 wt. %), reflecting the limited constraints on aenigmatite stability. These inaccuracies tend to be associated with volumetrically minor phases (e.g., aenigmatite and apatite: <5%, Field et al., 2013; Gleeson et al., 2017), and best-fit liquid lines of descent (Figure 3) capture the trend of natural samples over most of their differentiation.

4.2 Trace element trends

Each volcanic system exhibits extreme compatible (e.g., Sr) and incompatible (e.g., REE, Nb) trace element variation, consistent with protracted fractional crystallization (Figure 4). Zircon solubility in peralkaline melts is significantly higher than sub-alkaline melts (Watson, 1979), consequently Zr remains almost perfectly incompatible during differentiation in peralkaline rhyolites (Field et al., 2012a). Thus, we can use Zr as a marker of degree of magmatic evolution. In each panel of Figure 4 there is a near-continuous trend from primitive mafic lavas (lowest Zr, ~100 ppm) to silicic rocks (highest Zr, up to ~3000 ppm). Sr is compatible in both plagioclase and alkali feldspar and there is a clear distinction between the relatively high Sr contents of Erta Ale silicic rocks and the low concentrations elsewhere (Figure 4). Low Ba concentrations (<500 ppm) in rhyolites reflect alkali feldspar removal and are observed at all volcanic systems except Erta Ale, which lacks alkali feldspar (Figure 4; Bizouard et al., 1980). Silicic samples from Aluto have relatively high Ba (180–470 ppm), Gedemsa and Kone are similar in terms of their minima (~25 ppm) and pattern, while the lowest Ba values (~3 ppm) are observed at Dabbahu and Badi. Several silicic samples from Gedemsa with elevated Ba have previously been linked to alkali feldspar accumulation (Peccerillo et al., 2003).

The volcanic systems are characterized by subtly different but generally constant incompatible trace element ratios, e.g., Nb/Zr and Rb/Zr (Figure 4). They also exhibit clear distinctions in maximum incompatible element enrichment (Figure 4). The greatest incompatible element concentrations are observed at the MER volcanoes Kone (~2400 ppm Zr) and Gedemsa (~2300 ppm Zr), and the MHRS off-axis volcano Badi shows the largest range with maximum ~3000 ppm Zr. Zr contents of Erta Ale samples reach only ~750 ppm (Figure 4). Zr contents of Dabbahu samples reach 1300 ppm and divide into a high and low Nb series at ~700 ppm Zr. Dabbahu samples displaced to lower Nb values are comendites, possibly reflecting a greater role of ilmenite (which accommodates Nb) in their formation. However, we acknowledge that the P-T-fO_2 and compositional conditions that govern Fe-Ti oxide stability in peralkaline melts remain poorly understood (Marshall et al., 2009) and it is unclear what magmatic processes might favour ilmenite crystallization in these samples.

Y is positively correlated with Zr for all complexes except Badi, where several samples fall off the linear array (Figure 4), perhaps due to amphibole and/or apatite fractionation (c.f. White et al., 2009). Th is highly incompatible in peralkaline magmas (Martin and Sigmarsson, 2010) and samples from Dabbahu, Badi, Erta Ale and Aluto define near constant Th/Zr ratios. Gedemsa samples are scattered, with elevated Th/Zr and Pb/Zr across the compositional range, likely reflecting variability in the parental basalts (c.f. Giordano et al., 2014). At the rift-scale, minor differences in incompatible element ratios between the MER and Afar Rift may represent subtle differences in parental magmas between regions. Ratios sensitive to crustal assimilation of Pan-African basement (Rb/Nb, Figure 4) are low for Quaternary volcanic systems but clearly elevated for ~30 Ma ignimbrites (Ayalew et al., 2002).

4.3 Isotopic constraints

$\delta^{18}O$ results are presented in Figure 5a. We consider all $\delta^{18}O_{glass}$ values to be representative of melt composition and have used experimentally determined fractionation factors of Appora et al.

(2003) to estimate and plot $\delta^{18}O_{melt}$ from the measured $\delta^{18}O_{mineral}$ (olivine, quartz and feldspars). Erta Ale values after Barrat et al. (1998) are derived from whole-rock $\delta^{18}O$. As their crystal content is low (~20 % by volume, Field et al., 2012b) it is reasonable to assume that $\delta^{18}O_{whole\text{-}rock}$ provides a close approximation to $\delta^{18}O_{melt}$.

The vast majority of $\delta^{18}O$ values fall between 5 and 6.5 ‰, and lie within the range predicted by fractional crystallization of primitive rift-related magmas (shaded area, Figure 5a, detailed discussion in Section 5.1). High $\delta^{18}O_{melt}$ (>7.0 ‰) is observed in only three Quaternary samples: a Kone pre-caldera silicic sample; a Gedemsa alkali feldspar separated from a pre-caldera rhyolite and a Dabbahu comendite (Table 2). The most evolved samples from Erta Ale divide into two populations, with normal (5.5–6.4 ‰) and low $\delta^{18}O$ (down to 5.2 ‰, Barrat et al., 1998). New and published $\delta^{18}O_{olivine}$ data are within error of typical upper mantle values (5.2±0.2 ‰, Eiler, 2001). Further, $\delta^{18}O$ values for ~30 Ma ignimbrites (grey crosses, after Ayalew et al., 2002) show both normal and high $\delta^{18}O_{melt}$ groupings.

New Sr- and Nd-isotope results from the MHRS, Dabbahu and Badi are combined with previous analyses in Figure 5b. Sr-Nd isotopes are available for all systems except Aluto. ε_{Nd} values range from 6.52 to 0.92 with generally close agreement between the Nd-isotopic ratios for silicic and mafic samples from the same complex. Most samples fall within the Ethiopian mantle array (dashed black ellipse) although a number of silicic samples are elevated to more radiogenic $^{87}Sr/^{86}Sr$ values (up to 0.7072). Finally, Sr- and Nd-isotopic ratios for ~30 Ma basalts and ignimbrites from across Ethiopia show greater scatter and overlap with Pan-African crustal samples (Figure 5b).

5. Discussion

5.1 Fingerprinting crustal interactions: δ^{18}O constraints

Oxygen isotopes can provide valuable insights into magma-crust interactions. However, it is instructive to first consider how fractional crystallization affects the δ^{18}O of peralkaline magmas. Most δ^{18}O measurements from natural volcanic series show typical mantle-derived basalts have δ^{18}O of 5.2–5.8 ‰ (Eiler, 2001) with values increasing a little during fractional crystallization (Harris et al., 2000). We model the $\delta^{18}O_{melt}$ trajectory for peralkaline rhyolites in Ethiopia from Aluto and Dabbahu (Section 3.2) and find that evolved rhyolites should show a modest $\delta^{18}O_{melt}$ increase of ~0.6 ‰ during fractional crystallization from basalt (Figure 5a). The minor $\delta^{18}O_{melt}$ increase is explained because Rhyolite-MELTS predicts that the bulk (~80 %) of the fractionating assemblage comprises mineral phases (olivine, clinopyroxene and plagioclase) that have relatively small fractionation factors at temperatures of 1250–750 °C (Eiler, 2001).

The modelled $\delta^{18}O_{melt}$ trajectory is shaded in Figure 5a. We interpret samples that fall outside this range as having interacted with high or low δ^{18}O sources. We emphasize that the δ^{18}O of magmatic residue or cumulate phases overlaps with normal magmatic δ^{18}O and so interactions with these cannot be detected by δ^{18}O analyses (see Section 5.4). High δ^{18}O samples have assimilated Pan-African crustal rocks (Figure 1c) with δ^{18}O of 7–18 ‰ (Duffield et al., 1997; Ayalew et al., 2002) while low δ^{18}O samples have likely assimilated shallow hydrothermally-altered crustal rocks. We rule out a sub-solidus alteration or weathering cause for low δ^{18}O lavas because sampling targeted exceptionally fresh material without visible surface alteration (Barrat et al., 1998). Further, while in principle low δ^{18}O silicic magmas could be generated by fractional crystallization of low $\delta^{18}O$ mafic magmas, none of the basaltic samples or olivine separates (Table 2, Figure 5a) lie significantly outside typical upper mantle range (Section 4.2).

High-temperature hydrothermal circulation of low-$\delta^{18}O$ meteoric fluids at active volcanic systems causes alteration and generates low-$\delta^{18}O$ volcanic crust (Norton and Taylor, 1979). Geothermal activity is reported at all volcanic systems in the study, geothermal fluids and groundwater have $\delta^{18}O$ between –1 and –5 ‰ (Duffield et al., 1997; Darling et al., 1996), and at Aluto deep drilling has identified high temperatures (300–400 °C) and extensive hydrothermally-altered volcanic deposits (Teklemariam et al., 1996). To date, there are no $\delta^{18}O$ measurements of the hydrothermally-altered facies underlying Ethiopian volcanoes, however, a useful comparison can be made with well-studied geothermal systems in Iceland such as Krafla. Here, Pope et al. (2013) showed that shallow altered volcanic crust has values of –6 ‰, intermediate between unaltered basalts (~5.5 ‰) and geothermal fluids (–12 ‰). Unaltered Ethiopian basalts are also ~5.5 ‰ (Figure 5) and so assuming comparable levels of fluid-rock interaction to Iceland we estimate that Ethiopian hydrothermally-altered crust has $\delta^{18}O$ of 2 ‰ (we averaged all $\delta^{18}O$ values from Duffield et al., 1997 and Darling et al., 1996, above, to make a conservative estimate of –1.5 ‰ for geothermal fluids).

In Figure 5a, the horizontal lines above and below the grey shaded fractional crystallization $\delta^{18}O_{melt}$ trajectory indicate the percentage of melt sourced from crustal materials assuming end-member values of 2 ‰ (hydrothermally-altered volcanic crust) and 12 ‰ (Pan-African crust). Until detailed $\delta^{18}O$ studies of local crust are undertaken at each system (i.e., from xenoliths) our estimates of melt mass percentage serve guidelines rather than precise values.

5.2 Genesis of silicic melts in Quaternary magmatic segments

The $\delta^{18}O$ of Quaternary volcanic products from across Ethiopia generally fall between 5.0 and 6.5 ‰ and show a close correspondence with our modelled $\delta^{18}O_{melt}$ fractional crystallization trajectory (Figure 5a). The pantellerites show no oxygen-isotopic evidence for crustal assimilation, strongly suggesting that the most evolved silicic rocks of Ethiopia are not derived from melting of high-$\delta^{18}O$ Pan-African crust. This conclusion agrees with trace element evidence, for example, large ion lithophile element and high field strength element ratios (LILE/HFSE, e.g. Rb/Nb <1.5) which show only limited overlap with Pan-African (Figure 4, Peccerillo et al., 2003, 2007).

Subtle crustal assimilation signatures are detected in a limited number of Quaternary samples (Figure 5a), and Sr-Nd isotopes provide an additional test (Figure 5b). Sr concentrations in the silicic samples are very low (Figure 4) making Sr-isotopes very sensitive to crustal assimilation. In Figure 5b a simple binary mixing model is shown for a typical uncontaminated mantle-derived melt (white star) and a Pan-African lithosphere end-member (grey star, from Rooney et al., 2012c). The mixing curves demonstrate that for a typical pantelleritic melt (starting with 5 ppm Sr and 200 ppm Nd) addition of 5–10 % Pan-African material can displace $^{87}Sr/^{86}Sr$ to high crustal values without significantly altering ε_{Nd}. Thus, elevated $^{87}Sr/^{86}Sr$ observed in various silicic samples in Figure 5b are explained by relatively low levels of crustal assimilation (<10 %). This agrees with previous radiogenic isotope studies in the MER (e.g., Peccerillo et al., 2003; Giordano et al., 2014) that identified elevated $^{87}Sr/^{86}Sr$ in feldspar phenocrysts (up to ~0.7056) as well as whole-rock samples.

Together, the major and trace elements as well as the Sr-Nd-O isotopes and Rhyolite-MELTS models are consistent with fractional crystallization from basalts to rhyolites with very minimal crustal assimilation to explain the origins of Quaternary peralkaline magmas across Ethiopia. These observations agree with petrogenetic studies from other regions of continental extension, e.g., Taupo Volcanic Zone, where fractional crystallization is the primary mechanism of silicic magmagenesis (e.g., Graham et al. 1995; Deering et al., 2008).

The three high-$\delta^{18}O$ samples (Table 1) relate to pre-caldera phases of activity (samples GD22 and 2-11 from Gedemsa and Kone, respectively) and a period of comendite melt production following a hiatus in silicic activity (sample 011, Dabbahu). $\delta^{18}O$ data from Aluto do not follow a similar temporal trend as both pre-caldera (6.5 ‰) and early post-caldera comenditic samples (6.1 ‰) are very close to the recent post-caldera products (6.2–6.4 ‰). Detailed discussion on the origins of these high-$\delta^{18}O$ samples is beyond the scope of this study, although future isotopic investigations of glass and minerals from these outliers is desirable.

Although the key finding from our $\delta^{18}O$ analysis is that assimilation of Pan-African crustal materials is limited, our analyses also reveal that evidence for crustal assimilation is entirely absent in some systems. For example, no high-$\delta^{18}O$ lavas were found at Erta Ale, Aluto, or Badi (Figure 5a). Erta Ale is notable because it is in the most mature rift setting. Although magmatic flux and partial crustal melting are expected to be greatest here (Section 1), the absence of a high-$\delta^{18}O$ signal strongly suggests that earlier intrusions and crustal modification have effectively removed any fusible Pan-African crust. This hypothesis is consistent with geophysical evidence and is developed with petrological models for crustal modification in Section 5.4. An additional feature of the $\delta^{18}O$ data is that, despite large geothermal systems being present at each volcanic system studied, only at Erta Ale are low $\delta^{18}O$ silicic samples identified (trachytes, Figure 5a). In this case we suspect that hydrothermally-altered crust in the EAS (Figure 1a) might be more extensive and/or altered based on seismic interpretations indicating thicker rift fill (Figure 1c, Hammond et al., 2011) and the more mature rift morphology and pervasive faulting facilitating greater meteoric water ingress.

5.3 Geotectonic controls on melt evolution

Peralkaline magmas are a ubiquitous feature of silicic volcanism in Ethiopia. However, we identified clear variations in melt evolution between the volcanic systems. The most evolved peralkaline melts from Kone, Gedemsa, Aluto and Badi are similar in terms of their exceptional peralkalinity (NK/A >1.6, Figure 2b) and extreme incompatible element enrichment (e.g., Zr and Th, Figure 4). By comparison, pantellerites from Dabbahu volcano are less peralkaline (NK/A <1.6), with lower incompatible element concentrations, while at Erta Ale, silicic peralkaline melts are rare.

These observations beg the question: what drives extreme fractional crystallization, and what rift settings amplify these processes? In general, conditions that promote peralkaline rhyolite genesis are: (1) fractional crystallization of a transitional basalt, with an alkali content between those of tholeiitic and alkali basalts (Barberi et al., 1975); (2) low oxygen fugacity (NNO–1 or below; Scaillet and Macdonald 2001); (3) retention of a magmatic volatile phase which extends the crystallization interval to low pressures (≤150 MPa) and temperatures (≤750°C) (Macdonald, 1987; Macdonald et al., 2014).

The flux of magma into peralkaline volcanic systems also plays a key role promoting geochemical variations (Macdonald, 2012). At high magma fluxes, the elevated heat and mass input promotes homogenization, reducing the likelihood of reaching the extremes of fractional crystallization (Macdonald et al., 2014). Magmatic fluxes are difficult to quantify directly and so we calculate eruptive fluxes for each volcanic system, and make the reasonable assumption that these are proportional to magmatic flux. Erupted volumes are calculated from the volume of the edifice and caldera (where present) following methods of Hutchison et al. (2016a), and fluxes are estimated using available age constraints (summarized in Table 4). Clearly, flux estimates do not consider dykes and unerupted magmas, and so a necessary assumption is that intrusive:extrusive ratios are comparable for each volcanic setting. Further, due to the paucity of detailed mapping and geochemistry on individual silicic centres along the EAS we did not estimate their volumes. Instead, we treat the segment as a single volcanic system; this is justified because the Erta Ale range has smooth along-axis topography (analogous to a single shield volcano) and the eruptive centres show clear evidence for magmatic interconnectivity (Pagli et al., 2012; Xu et al., 2017).

Eruptive volumes and fluxes are plotted in Figure 6a-b and reflect variations in mantle melt productivity as well as crustal melt storage. The greatest eruptive volumes (~400 km^3) are associated with Erta Ale. For the MHRS, although Dessisa et al. (2013) and Medynski et al. (2015) have reported magnetotelluric and geochemical evidence for an off-axis mantle magma reservoir developing beneath Badi over the last ~30 ka, our volume estimates suggest that over longer (>100 ka) timescales the eruptive fluxes have been greater at on-axis Dabbahu, compared to off-axis Badi. In the MER, eruptive volumes increase southwards with the greatest fluxes associated with Aluto (Figure 6b, Table 4). Although one might expect magmatic fluxes to increase northwards along the MER, and correlate with increasing rift maturity, seismic tomography (Gallacher et al., 2016) reveals that the lowest velocities (i.e. greatest mantle melt production) are associated with the central MER (beneath the Aluto-Gedemsa segment) rather than Kone and more northern MER segments. Comparing eruptive volumes and fluxes with geochemical indicators of melt evolution (e.g., Zr concentration, Figure 6c) we find that volcanic systems with the lowest eruptive fluxes (i.e., Badi, Kone and Gedemsa, 0.05–0.2 km^3 ka^{-1}) have the most evolved magmas.

Rift maturity is one of the main controls on melt evolution and this is demonstrated in nascent seafloor spreading settings like Erta Ale. Here, the lithosphere is extensively thinned and enhanced decompression melting (Bastow and Keir, 2011) generates parental basalts that are tholeiitic (Figure 2a) and therefore unable to generate evolved peralkaline rhyolites (White et al., 2009). In contrast, parental melts in the MER and MHRS of Afar are transitional basalts (Figures 2a, 4) and since Rhyolite-MELTS models (Table 3) suggest similar magma storage conditions we look to other explanations for differences in peralkalinity between these systems.

Our analysis of eruptive volumes strongly suggests that local magmatic flux is also an important control on peralkalinity (Figure 6c). Hence the more chemically-evolved nature of the MER volcanoes and off-axis Badi compared to those of on-axis Dabbahu results from the higher magma flux on the MHRS axis. As outlined above, variations in local magma supply reflect spatial variations in mantle magma productivity and/or variations in crustal melt storage. In the second case it is well known that variations in rift structures and stress field play an important role in magma ascent and storage (e.g., Maccaferri et al., 2014). Protracted magma storage will promote fractionation and melt evolution, but will also favour cooling and degassing making the magma less likely to erupt.

In the MHRS, mantle melt production does not appear to be enhanced beneath the rift-axis (Dessisa et al., 2013) and so we suggest that at Badi the magma supply is lower because off-axis magma plumbing systems are less well-developed (i.e., crustal structures and/or stress field inhibit magma ascent). Thus off-axis melts at Badi are more likely to stall throughout the crust, decreasing melt supply to peralkaline magma reservoirs, which ultimately reduces homogenization and promotes more extreme fractionation. In the MER, regions of thicker crust do not amplify peralkalinity (e.g., Aluto, Figure 6c) and so we suggest that local magma supply in the MER indicates variations in mantle melt productivity. Thus melt production is greatest in the central MER beneath the Aluto-Gedemsa segment (in agreement with seismic tomography, Gallacher et al., 2016) and this reduces melt evolution compared to Kone. In summary, settings where the parental basalts are transitional in composition, and where local magmatic and thermal fluxes are low, will promote extreme melt evolution (Figure 6d).

5.4 Crustal modification

A corollary of our conclusion that fractional crystallization is the main driver of silicic magmagenesis is that large volumes of crystal cumulate are generated and stored within the crust. Estimates of cumulate volumes can be made from incompatible element contents of whole-rock samples and Rhyolite-MELTS models. Since Zr is completely incompatible (Field et al., 2012a) we use it as a proxy for melt fraction ($F = Zr_{parent} / Zr_{sample}$), assuming the most primitive basalt at each volcano represents parental magma. Using Rhyolite-MELTS we predict cumulate phase proportions at each fractionation and temperature step, and so by using the Zr constrained melt fraction (F) it is possible to place all samples (from basalt to peralkaline rhyolite) on the Rhyolite-MELTS liquid line of descent and evaluate the crystallizing minerals and their volumes. From eruptive volume estimates (Section 5.3), and assuming sample suites from each volcano are representative, we estimate cumulate volumes and fluxes (Figure 6a-b, Table 4).

Our calculations demonstrate that the volcanic systems generate large cumulate bodies (100–450 km^3, Figure 6a) and that the silicic complexes of the MER and MHRS will have cumulate volumes 3–5 times greater than the erupted volume (Table 4). At Erta Ale, where volcanic products are much less evolved and dominated by mafic samples (Figure 2a), we find that more material is erupted than forms cumulate (i.e., cumulate volume:erupted volume is 0.5, Table 4).

Magmatic cumulates must be accommodated in the extending crust. For each volcanic system we have calculated the space created by rift extension (using the crustal thickness, extension rate and the along-axis length of the system) and have compared this to the volume of cumulates needed to balance the erupted volumes. The comparison is shown in the final column of Table 4 (ratio of cumulate volume to total space created by extension). For the axial volcanoes of the MER and MHRS of Afar we calculate that 16–30 % of the volume generated by crustal extension beneath a silicic complex would be filled by magmatic cumulates. This is a considerable volume and we stress that this is a minimum because the volume fluxes do not account for unerupted (intrusive) melts (Section 5.3). Recent mafic dyking sequences in the MHRS (Ferguson et al., 2010), suggest intrusive:extrusive ratios of between 5:1 and 10:1 and so dykes and sills will also play a major role in crustal modification at the magmatic segments.

Our petrological estimates of cumulate volumes have clear geophysical consequences and it is important to underscore that there is abundant seismic evidence for large volumes of mid-crustal intrusions beneath the magmatic segments of the MER and Afar (Keranen et al., 2004; Mackenzie et al., 2005). Gravity surveys require high-density bodies (3000–3100 kg m^3, Markris and Ginzburg, 1987; Cornwell et al, 2006; Lewi et al., 2016) to be present beneath the magmatic segments as well as the silicic complexes (including Gedemsa, Mahatsente et al., 1999). In fact, the bulk densities we calculated with Rhyolite-MELTS for cumulates (~3050 kg m^3, Table 3) are remarkably similar to the gravity-derived densities.

Geophysical and petrological evidence reinforce the notion that large volumes of the Ethiopian crust beneath the magmatic rift segments comprise magmatic intrusions and cumulates. An interesting observation from the cumulate volumes (Table 4) is that at Erta Ale only ~1 % of the volume generated due to rift extension is filled by cumulates. This implies that extension in the EAS must be accommodated by greater levels of dyking and/or plate stretching than in the MER/MHRS. Although our petrological observations cannot discriminate between these two alternatives, seismic evidence (Bastow and Keir, 2011) clearly supports the latter revealing that the plate is abruptly thinned beneath the EAS (Figure 1c). Thus, both rift structure (from seismic) and cumulate volumes (from magma chemistry) can be used to infer a greater role of plate stretching in mature rifts at the onset of sea-floor spreading.

Finally, our interpretation that the Ethiopian crust has been substantially modified by magmatic intrusions explains why $\delta^{18}O$ evidence for Pan-African crustal assimilation is so limited (Section 5.2). ~45 Ma of magmatism in the region has likely removed or assimilated most fusible crustal contaminants, and the active segments are predominantly composed of magmatic cumulates that have $\delta^{18}O$ indistinguishable from the more recent mantle-derived melts, except in rare cases where hydrothermal alteration has subsequently lowered $\delta^{18}O$. We suggest that $\delta^{18}O$ of silicic magmas should converge to mantle values during rift evolution. Such a secular trend in crustal contamination has been observed in MER mafic samples (Rooney et al., 2007) and intriguingly the limited $\delta^{18}O$ data from ignimbrites associated with flood basalt volcanism at ~30 Ma (Ayalew et al., 2002) include some examples with exceptionally high $\delta^{18}O$ (Figure 5a) and low ε_{Nd} (Figure 5b), consistent with greater availability of crustal contaminants in earlier phases of rifting.

6. Conclusions

Silicic volcanic rocks in Ethiopia provide important insights into how magmas evolve and interact with the crust during continental break-up. Magmas of Quaternary age show little geochemical evidence for interaction with Pan-African crust. They generally have $\delta^{18}O$ of 5.5–6.5 ‰, independent of variations in crustal thickness (15–40 km), extension rates (5–15 mm a^{-1}) and eruptive fluxes (0.05–0.4 km^3 ka^{-1}). Sr-Nd isotopes and trace element systematics confirm that geochemical diversity of these young silicic magmas primarily reflects variations in extent of fractional crystallization.

Peralkaline magmas associated with ancient rift zones have generated many of the world's largest REE deposits and a major challenge for exploration geologists is to identify the geotectonic settings that host economically significant ore bodies (Goodenough et al., 2016). Our analyses suggest that the two most important controls on melt evolution, and hence REE enrichment, are rift maturity and local magma supply (Section 5.3). Thus intermediate-mature continental rifts (i.e., MER and MHRS of Afar) where parental magmas are transitional rather than tholeiitic, and where local magma supply is reduced (due to lower mantle melt productivity, e.g., Kone, and/or crustal structures or stress field inhibiting magma ascent, e.g., off-axis Badi) offer the best settings for differentiation and melt peralkalinity. Early phases of rift development might also be sufficient for generating evolved peralkaline melts, however, caution is required because in Ethiopia the high magmatic fluxes associated with ~30 Ma flood basalts and ignimbrites likely did not allow silicic melts to evolve to the same extent as many Quaternary settings (Figure 4). Our study underscores that ancient rift zones that have reached and preserved an intermediate-mature phase of development, ideally with off-axis volcanism, should provide excellent prospects for major REE deposits.

Acknowledgments, Samples, and Data

This work was supported by the RiftVolc project (NE/L013932/1, Rift volcanism: past, present and future) and a NERC studentship (NE/J5000045/1) awarded to W.H. W.H. also received funding from the European Union’s Horizon 2020 research and innovation programme under grant agreement No. 689909. C. V-B. and I. M. acknowledge a BGS-NIGL Programme Project (40227) for Sr-Nd-Pb isotope analysis of the four samples from Dabbahu. C.V-B. publishes with permission of the Executive Director of the British Geological Survey (NERC). Oxygen isotope analysis at SUERC was supported by a NERC Stable Isotope Facility grant (IP-1367-0513). Technical assistance at SUERC was provided by A. MacDonald and T. Donnely. J. Blusztajn assisted with the isotopic measurements at Woods Hole Oceanographic Institution. We thank L.

Field, S. Medynski and M. Rampey for providing samples and A. Peccerillo for providing clarification on previous geochemical data. J. Biggs provided valuable comments on an earlier version of the manuscript. We also thank Tyrone Rooney and Özge Karakas for thorough, constructive reviews and Mike Bickle for editorial handling.

References

Agostini, A., Bonini, M., Corti, G., Sani, F., Mazzarini, F., 2011. Fault architecture in the Main Ethiopian Rift and comparison with experimental models: Implications for rift evolution and Nubia–Somalia kinematics. Earth Planet. Sci. Lett. 301, 479–492. doi:10.1016/j.epsl.2010.11.024

Annen, C., Blundy, J.D., Sparks, R.S.J., 2006. The genesis of intermediate and silicic magmas in deep crustal hot zones. J. Petrol. 47, 505–539. doi:10.1093/petrology/egi084

Appora, I., Eiler, J.M., Matthews, A., Stolper, E.M., 2003. Experimental determination of oxygen isotope fractionations between CO_2 vapor and soda-melilite melt. Geochim. Cosmochim. Acta 67, 459–471. doi:10.1016/S0016-7037(02)01090-6

Armitage, J.J., Ferguson, D.J., Goes, S., Hammond, J.O.S., Calais, E., Rychert, C.A., Harmon, N., 2015. Upper mantle temperature and the onset of extension and break-up in Afar, Africa. Earth Planet. Sci. Lett. 418, 78–90. doi:10.1016/j.epsl.2015.02.039

Ayalew, D., Barbey, P., Marty, B., Reisberg, L., Yirgu, G., Pik, R., 2002. Source, genesis, and timing of giant ignimbrite deposits associated with Ethiopian continental flood basalts. Geochim. Cosmochim. Acta 66, 1429–1448. doi:10.1016/S0016-7037(01)00834-1

Ayalew, D., Yirgu, G., 2003. Crustal contribution to the genesis of Ethiopian plateau rhyolitic ignimbrites: basalt and rhyolite geochemical provinciality. J. Geol. Soc. London. 160, 47–56. doi:10.1144/0016-764901-169

Ayalew, D., Jung, S., Romer, R.L., Kersten, F., Pfänder, J.A., Garbe-Schönberg, D., 2016. Petrogenesis and origin of modern Ethiopian rift basalts: Constraints from isotope and trace element geochemistry. Lithos 258–259, 1–14. doi:10.1016/j.lithos.2016.04.001

Barberi, F., Ferrara, G., Santacroce, R., Treuil, M., Varet, J., 1975. A transitional basalt-pantellerite sequence of fractional crystallization, the Boina Centre (Afar Rift, Ethiopia). J. Petrol. 16, 22–56. doi:10.1093/petrology/16.1.22

Barberi, F., Tazieff, H., Varet, J., 1972. Volcanism in the Afar Depression: Its Tectonic and Magmatic Significance. Dev. Geotecton. 7, 19–29. doi:10.1016/B978-0-444-41087-0.50007-5

Barberi, F., Varet, J., 1970. The Erta Ale volcanic range (Danakil Depression, northern Afar, Ethiopia). Bull. Volcanol. 34, 848–917. doi:10.1007/BF02596805

Barrat, J.A., Fourcade, S., Jahn, B.M., Cheminée, J.L., Capdevila, R., 1998. Isotope (Sr, Nd, Pb, O) and trace-element geochemistry of volcanics from the Erta' Ale range (Ethiopia). J. Volcanol. Geotherm. Res. 80, 85–100. doi:10.1016/S0377-0273(97)00016-4

Barrat, J.A., Joron, J.L., Taylor, R.N., Fourcade, S., Nesbitt, R.W., Jahn, B.M., 2003. Geochemistry of basalts from Manda Hararo, Ethiopia: LREE-depleted basalts in Central Afar. Lithos 69, 1–13. doi:10.1016/S0024-4937(03)00044-6

Bastow, I.D., Keir, D., 2011. The protracted development of the continent–ocean transition in Afar. Nat. Geosci. 4, 248–250. doi:10.1038/ngeo1095

Beyene, A., Abdelsalam, M.G., 2005. Tectonics of the Afar Depression: A review and synthesis. J. African Earth Sci. 41, 41–59. doi:10.1016/j.jafrearsci.2005.03.003

Bialas, R.W., Buck, W.R., Qin, R., 2010. How much magma is required to rift a continent? Earth Planet. Sci. Lett. 292, 68–78. doi:10.1016/j.epsl.2010.01.021

Bindeman, I.N., Ponomareva, V. V., Bailey, J.C., Valley, J.W., 2004. Volcanic arc of Kamchatka: a province with high-$\delta^{18}O$ magma sources and large-scale $^{18}O/^{16}O$ depletion of the upper crust. Geochim. Cosmochim. Acta 68, 841–865. doi:10.1016/j.gca.2003.07.009

Bizouard, H., Barberi, F., Varet, J., 1980. Mineralogy and petrology of Erta Ale and Boina volcanic series, Afar Rift, Ethiopia. J. Petrol. 21, 401–436. doi:10.1093/petrology/21.2.401

Bucholz, C.E., Jagoutz, O., VanTongeren, J.A., Setera, J., Wang, Z., 2017. Oxygen isotope trajectories of crystallizing melts: Insights from modeling and the plutonic record. Geochim. Cosmochim. Acta 207, 154–184. doi:10.1016/j.gca.2017.03.027

Buck, W.R., 2006. The role of magma in the development of the Afro-Arabian Rift System. Geol. Soc. London, Spec. Publ. 259, 43–54. doi:10.1144/GSL.SP.2006.259.01.05

Cornwell, D.G., Mackenzie, G.D., England, R.W., Maguire, P.K.H., Asfaw, L.M., Oluma, B., 2006. Northern Main Ethiopian Rift crustal structure from new high-precision gravity data. Geol. Soc. London, Spec. Publ. doi:10.1144/GSL.SP.2006.259.01.23

d'Acremont, E., Leroy, S., Beslier, M.-O., Bellahsen, N., Fournier, M., Robin, C., Maia, M., Gente, P., 2005. Structure and evolution of the eastern Gulf of Aden conjugate margins from seismic reflection data. Geophys. J. Int. 160, 869–890. doi:10.1111/j.1365-246X.2005.02524.x

Darling, W.G., Gizaw, B., Arusei, M.K., 1996. Lake-groundwater relationships and fluid-rock interaction in the East African Rift Valley: isotopic evidence. J. African Earth Sci. 22, 423–431. doi:10.1016/0899-5362(96)00026-7

Deering, C.D., Cole, J.W., Vogel, T.A., 2008. A rhyolite compositional continuum governed by lower crustal source conditions in the taupo volcanic zone, New Zealand. J. Petrol. 49, 2245–2276. doi:10.1093/petrology/egn067

Desissa, M., Johnson, N.E., Whaler, K.A., Hautot, S., Fisseha, S., Dawes, G.J.K., 2013. A mantle magma reservoir beneath an incipient mid-ocean ridge in Afar, Ethiopia. Nat. Geosci. 6, 861–865. doi:10.1038/ngeo1925

Dufek, J., Bergantz, G.W., 2005. Lower crustal magma genesis and preservation: a stochastic framework for the evaluation of basalt–crust interaction. J. Petrol. 46, 2167–2195.

Duffield, W.A., Bullen, T.D., Clynne, M.A., Fournier, R.O., Janik, C.J., Lanphere, M.A., Lowenstern, J., Smith, J.G., Giorgis, L.W., Kahsai, G., 1997. Geothermal potential of the Alid volcanic center, Danakil Depression, Eritrea. US Geological Survey, Open File Report 97–291.

Ebinger, C., 2005. Continental break-up: the East African perspective. Astron. Geophys. 46, 2.16-2.21. doi:10.1111/j.1468-4004.2005.46216.x

Ebinger, C.J., Casey, M., 2001. Continental breakup in magmatic provinces: An Ethiopian example. Geology 29, 527–530. doi:10.1130/0091-7613(2001)029<0527:CBIMPA>2.0.CO;2

Eiler, J.M., 2001. Oxygen Isotope Variations of Basaltic Lavas and Upper Mantle Rocks. Rev. Mineral. Geochemistry 43, 319–364. doi:10.2138/gsrmg.43.1.319

Ferguson, D.J., Barnie, T.D., Pyle, D.M., Oppenheimer, C., Yirgu, G., Lewi, E., Kidane, T., Carn, S., Hamling, I., 2010. Recent rift-related volcanism in Afar, Ethiopia. Earth Planet. Sci. Lett. 292, 409–418. doi:10.1016/j.epsl.2010.02.010

Ferguson, D.J., Maclennan, J., Bastow, I.D., Pyle, D.M., Jones, S.M., Keir, D., Blundy, J.D., Plank, T., Yirgu, G., 2013a. Melting during late-stage rifting in Afar is hot and deep. Nature 499, 70–3. doi:10.1038/nature12292

Ferguson, D.J., Calvert, A.T., Pyle, D.M., Blundy, J.D., Yirgu, G., Wright, T.J., 2013b. Constraining timescales of focused magmatic accretion and extension in the Afar crust using lava geochronology. Nat. Commun. 4, 1416. doi:10.1038/ncomms2410

Field, L., Blundy, J., Brooker, R. A., Wright, T., Yirgu, G., 2012a. Magma storage conditions beneath Dabbahu Volcano (Ethiopia) constrained by petrology, seismicity and satellite geodesy. Bull. Volcanol. doi:10.1007/s00445-012-0580-6

Field, L., Barnie, T., Blundy, J., Brooker, R.A., Keir, D., Lewi, E., Saunders, K., 2012b. Integrated field, satellite and petrological observations of the November 2010 eruption of Erta Ale. Bull. Volcanol. 74, 2251–2271. doi:10.1007/s00445-012-0660-7

Field, L., Blundy, J., Calvert, A., Yirgu, G., 2013. Magmatic history of Dabbahu, a composite volcano in the Afar Rift, Ethiopia. Bull. Geol. Soc. Am. 125, 128–147. doi:10.1130/B30560.1

Furman, T., Bryce, J., Rooney, T.O., Hanan, B., Yirgu, G., Ayalew, D., 2006. Heads and tails: 30 million years of the Afar plume. Geol. Soc. London, Spec. Publ. 259, 95–119.

Gallacher, R.J., Keir, D., Harmon, N., Stuart, G., Leroy, S., Hammond, J.O.S., Kendall, J.-M., Ayele, A., Goitom, B., Ogubazghi, G., Ahmed, A., 2016. The initiation of segmented buoyancy-driven melting during continental breakup. Nat. Commun. 7, 13110. doi:10.1038/ncomms13110

Giordano, F., D'Antonio, M., Civetta, L., Tonarini, S., Orsi, G., Ayalew, D., Yirgu, G., Dell'Erba, F., Di Vito, M. A., Isaia, R., 2014. Genesis and evolution of mafic and felsic magmas at Quaternary volcanoes within the Main Ethiopian Rift: Insights from Gedemsa and Fanta 'Ale complexes. Lithos 188, 130–144. doi:10.1016/j.lithos.2013.08.008

Gleeson, M.L.M., Stock, M.J., Pyle, D.M., Mather, T.A., Hutchison, W., Yirgu, G., Wade, J., 2017. Constraining magma storage conditions at a restless volcano in the Main Ethiopian Rift using phase equilibria models. J. Volcanol. Geotherm. Res. 337, 44–61. doi:10.1016/j.jvolgeores.2017.02.026

Goodenough, K.M., Schilling, J., Jonsson, E., Kalvig, P., Charles, N., Tuduri, J., Deady, E.A., Sadeghi, M., Schiellerup, H., Müller, A., Bertrand, G., Arvanitidis, N., Eliopoulos, D.G., Shaw, R.A., Thrane, K., Keulen, N., 2016. Europe's rare earth element resource potential: An overview of REE metallogenetic provinces and their geodynamic setting. Ore Geol. Rev. 72, 838–856. doi:10.1016/j.oregeorev.2015.09.019

Graham, I.J., Cole, J.W., Briggs, R.M., Gamble, J.A., Smith, I.E.M., 1995. Petrology and petrogenesis of volcanic rocks from the Taupo Volcanic Zone: a review. J. Volcanol. Geotherm. Res. 68, 59–87. doi:10.1016/0377-0273(95)00008-I

Gualda, G.A.R., Ghiorso, M.S., Lemons, R. V., Carley, T.L., 2012. Rhyolite-MELTS: A modified calibration of MELTS optimized for silica-rich, fluid-bearing magmatic systems. J. Petrol. 53, 875–890. doi:10.1093/petrology/egr080

Hammond, J.O.S., Kendall, J.M., Stuart, G.W., Keir, D., Ebinger, C., Ayele, A., Belachew, M., 2011. The nature of the crust beneath the Afar triple junction: Evidence from receiver functions. Geochemistry, Geophys. Geosystems 12. doi:10.1029/2011GC003738

Harris, C., Smith, S.H., le Roex, A.P., 2000. Oxygen isotope composition of phenocrysts from Tristan da Cunha and Gough Island lavas: variation with fractional crystallization and evidence for assimilation. Contrib. to Mineral. Petrol. 138, 164–175. doi:10.1007/s004100050015

Hayward, N.J., Ebinger, C.J., 1996. Variations in the along-axis segmentation of the Afar Rift system. Tectonics 15, 244. doi:10.1029/95TC02292

Hofmann, C., Courtillot, V., Féraud, G., Rochette, P., Yirgu, G., Ketefo, E., Pik, R., 1997. Timing of the Ethiopian flood basalt event and implications for plume birth and global change. Nature 389, 838–841. doi:10.1038/39853

Hutchison, W., Fusillo, R., Pyle, D.M., Mather, T.A., Blundy, J.D., Biggs, J., Yirgu, G., Cohen, B.E., Brooker, R.A., Barfod, D.N., Calvert, A.T., 2016a. A pulse of mid-Pleistocene rift volcanism in Ethiopia at the dawn of modern humans. Nat. Commun. 7, 13192. doi:10.1038/ncomms13192

Hutchison, W., Biggs, J., Mather, T.A., Pyle, D.M., Lewi, E., Yirgu, G., Caliro, S., Chiodini, G., Clor, L.E., Fischer, T.P., 2016b. Causes of unrest at silicic calderas in the East African Rift: New constraints from InSAR and soil-gas chemistry at Aluto volcano, Ethiopia. Geochemistry, Geophys. Geosystems 17, 3008–3030. doi:10.1002/2016GC006395

Hutchison, W., Pyle, D.M., Mather, T.A., Yirgu, G., Biggs, J., Cohen, B.E., Barfod, D.N., Lewi, E., 2016c. The eruptive history and magmatic evolution of Aluto volcano: new insights into silicic peralkaline volcanism in the Ethiopian rift. J. Volcanol. Geotherm. Res. 328, 9–33. doi:10.1016/j.jvolgeores.2016.09.010

Irvine, T.N., Baragar, W.R.A., 1971. A Guide to the Chemical Classification of the Common Volcanic Rocks. Can. J. Earth Sci. 8, 523–548. doi:10.1139/e71-055

Karakas, O., Dufek, J., 2015. Melt evolution and residence in extending crust: Thermal modeling of the crust and crustal magmas. Earth Planet. Sci. Lett. 425, 131–144. doi:10.1016/j.epsl.2015.06.001

Keir, D., Bastow, I.D., Corti, G., Mazzarini, F., Rooney, T.O., 2015. The origin of along-rift variations in faulting and magmatism in the Ethiopian Rift. Tectonics 34, 464–477. doi:10.1002/2014TC003698

Keranen, K., Klemperer, S.L., Gloaguen, R., EAGLE Working Group, 2004. Three-dimensional seismic imaging of a protoridge axis in the Main Ethiopian rift. Geology 32, 949. doi:10.1130/G20737.1

Lahitte, P., Gillot, P.-Y., Kidane, T., Courtillot, V., Bekele, A., 2003. New age constraints on the timing of volcanism in central Afar, in the presence of propagating rifts. J. Geophys. Res. Solid Earth 108. doi:10.1029/2001JB001689

Lewi, E., Keir, D., Birhanu, Y., Blundy, J., Stuart, G., Wright, T., Calais, E., 2016. Use of a high-precision gravity survey to understand the formation of oceanic crust and the role of melt at the southern Red Sea rift in Afar, Ethiopia. Geol. Soc. London, Spec. Publ. 420, 165–180. doi:10.1144/SP420.13

Macaulay, C.I., Fallick, A. E., Haszeldine, R.S., Graham, C.M., 2000. Methods of laser-based stable isotope measurement applied to diagenetic cements and hydrocarbon reservoir quality. Clay Miner. 35, 313–313. doi:10.1180/000985500546684

Maccaferri, F., Rivalta, E., Keir, D., Acocella, V., 2014. Off-rift volcanism in rift zones determined by crustal unloading. Nat. Geosci. 7, 297–300. doi:10.1038/ngeo2110

Macdonald, R., 1974. Nomenclature and petrochemistry of the peralkaline oversaturated extrusive rocks. Bull. Volcanol. 38, 498–516. doi:10.1007/BF02596896

Macdonald, R., 2012. Evolution of peralkaline silicic complexes: Lessons from the extrusive rocks. Lithos 152, 11–22. doi:10.1016/j.lithos.2012.01.014

Macdonald, R., Davies, G.R., Bliss, C.M., Leat, P.T., Bailey, D.K., Smith, R.L., 1987. Geochemistry of high-silica peralkaline rhyolites, Naivasha, Kenya rift valley. J. Petrol. 28, 979–1008. doi:10.1093/petrology/28.6.979

Macdonald, R., Belkin, H.E., Fitton, J.G., Rogers, N.W., Nejbert, K., Tindle, A.G., Marshall, A.S., 2008. The roles of fractional crystallization, magma mixing, crystal mush remobilization and volatile-melt interactions in the genesis of a young basalt-peralkaline rhyolite suite, the greater Olkaria volcanic complex, Kenya Rift valley. J. Petrol. 49, 1515–1547. doi:10.1093/petrology/egn036

Macdonald, R., Bagiński, B., Upton, B.G.J., 2014. The volcano-pluton interface; The Longonot (Kenya) and Kûngnât (Greenland) peralkaline complexes. Lithos 196–197, 232–241. doi:10.1016/j.lithos.2014.03.009

Mackenzie, G.D., Thybo, H., Maguire, P.K.H., 2005. Crustal velocity structure across the Main Ethiopian Rift: results from two-dimensional wide-angle seismic modelling. Geophys. J. Int. 162, 994–1006. doi:10.1111/j.1365-246X.2005.02710.x

Maguire, P.K.H., Keller, G.R., Klemperer, S.L., Mackenzie, G.D., Keranen, K., Harder, S., O’Reilly, B., Thybo, H., Asfaw, L., Khan, M.A., Amha, M., 2006. Crustal structure of the northern Main Ethiopian Rift from the EAGLE controlled-source survey; a snapshot of incipient lithospheric break-up. Geol. Soc. London, Spec. Publ. 259, 269–292. doi:10.1144/GSL.SP.2006.259.01.21

Mahatsente, R., Jentzsch, G., Jahr, T., 1999. Crustal structure of the Main Ethiopian Rift from gravity data: 3-dimensional modeling. Tectonophysics 313, 363–382. doi:10.1016/S0040-1951(99)00213-9

Makris, J., Ginzburg, A., 1987. The Afar Depression: transition between continental rifting and sea-floor spreading. Tectonophysics 141, 199–214. doi:10.1016/0040-1951(87)90186-7

Marshall, A.S., MacDonald, R., Rogers, N.W., Fitton, J.G., Tindle, A.G., Nejbert, K., Hinton, R.W., 2009. Fractionation of peralkaline silicic magmas: The greater olkaria volcanic complex, Kenya Rift Valley. J. Petrol. 50, 323–359. doi:10.1093/petrology/egp001

Martin, E., Sigmarsson, O., 2010. Thirteen million years of silicic magma production in Iceland: Links between petrogenesis and tectonic settings. Lithos 116, 129–144. doi:10.1016/j.lithos.2010.01.005

Medynski, S., Pik, R., Burnard, P., Vye-Brown, C., France, L., Schimmelpfennig, I., Whaler, K., Johnson, N., Benedetti, L., Ayelew, D., Yirgu, G., 2015. Stability of rift axis magma reservoirs: Spatial and temporal evolution of magma supply in the Dabbahu rift segment (Afar, Ethiopia) over the past 30 kyr. Earth Planet. Sci. Lett. 409, 278–289. doi:10.1016/j.epsl.2014.11.002

Medynski, S., Pik, R., Burnard, P., Williams, a., Vye-Brown, C., Ferguson, D., Blard, P.H., France, L., Yirgu, G., Seid, J.I., Ayalew, D., Calvert, A., 2013. Controls on magmatic cycles and development of rift topography of the Manda Hararo segment (Afar, Ethiopia): Insights from cosmogenic ^{3}He investigation of landscape evolution. Earth Planet. Sci. Lett. 367, 133–145. doi:10.1016/j.epsl.2013.02.006

Norton, D., Taylor, H.P., 1979. Quantitative simulation of the hydrothermal systems of crystallizing magmas on the basis of transport theory and oxygen isotope data: An analysis of the Skaergaard intrusion. J. Petrol. 20, 421–486. doi:10.1093/petrology/20.3.421

Pagli, C., Wright, T.J., Ebinger, C.J., Yun, S.-H., Cann, J.R., Barnie, T., Ayele, A., 2012. Shallow axial magma chamber at the slow-spreading Erta Ale Ridge. Nat. Geosci. 5, 284–288. doi:10.1038/ngeo1414

Peccerillo, A., Barberio, M.R., Yirgu, G., Ayalew, D., Barbieri, M., Wu, T.W., 2003. Relationships between Mafic and Peralkaline Silicic Magmatism in Continental Rift Settings: a Petrological, Geochemical and Isotopic Study of the Gedemsa Volcano, Central Ethiopian Rift. J. Petrol. 44, 2003–2032. doi:10.1093/petrology/egg068

Peccerillo, A., Donati, C., Santo, A., Orlando, A., 2007. Petrogenesis of silicic peralkaline rocks in the Ethiopian rift: geochemical evidence and volcanological implications. J. African Earth 48, 161–173. doi:10.1016/j.jafrearsci.2006.06.010

Peccerillo, A., Mandefro, B., Solomon, G., Bedru, H., Tesfaye, K., 1998. The Precambrian rocks from Southern Ethiopia: petrology, geochemistry and their interaction with the recent volcanism from the Ethiopian Rift Valley. Neues Jahrb. für Mineral. 237–262.

Pope, E.C., Bird, D.K., Arnórsson, S., 2013. Evolution of low-18O Icelandic crust. Earth Planet. Sci. Lett. 374, 47–59. doi:10.1016/j.epsl.2013.04.043

Rampey, M.L., 2005. The geology of the Kone volcanic complex, Ethiopia. University of Cambridge, PhD Thesis.

Rampey, M.L., Oppenheimer, C., Pyle, D.M., Yirgu, G., 2014. Journal of African Earth Sciences Physical volcanology of the Gubisa Formation, Kone Volcanic Complex, Ethiopia. J. African Earth Sci. 96, 212–219. doi:10.1016/j.jafrearsci.2014.04.009

Rampey, M.L., Oppenheimer, C., Pyle, D.M., Yirgu, G., 2010. Caldera-forming eruptions of the Quaternary Kone Volcanic Complex, Ethiopia. J. African Earth Sci. 58, 51–66. doi:10.1016/j.jafrearsci.2010.01.008

Rooney, T., Furman, T., Bastow, I., Ayalew, D., Yirgu, G., 2007. Lithospheric modification during crustal extension in the Main Ethiopian Rift. J. Geophys. Res. 112. doi:10.1029/2006JB004916

Rooney, T.O., 2017. The Cenozoic magmatism of East-Africa: Part I — Flood basalts and pulsed magmatism. Lithos 286–287, 264–301. doi:10.1016/j.lithos.2017.05.014

Rooney, T.O., Herzberg, C., Bastow, I.D., 2012a. Elevated mantle temperature beneath East Africa. Geology 40, 27–30. doi:10.1130/G32382.1

Rooney, T.O., Hart, W.K., Hall, C.M., Ayalew, D., Ghiorso, M.S., Hidalgo, P., Yirgu, G., 2012b. Peralkaline magma evolution and the tephra record in the Ethiopian Rift. Contrib. to Mineral. Petrol. 164, 407–426. doi:10.1007/s00410-012-0744-6

Rooney, T.O., Hanan, B.B., Graham, D.W., Furman, T., Blichert-toft, J., Schilling, J.G., 2012c. Upper mantle pollution during Afar plume-continental rift interaction. J. Petrol. 53, 365–389. doi:10.1093/petrology/egr065

Saria, E., Calais, E., Stamps, D.S., Delvaux, D., Hartnady, C.J.H., 2014. Present-day kinematics of the East African Rift. J. Geophys. Res. Solid Earth 119, 3584–3600. doi:10.1002/2013JB010901

Scaillet, B., Macdonald, R., 2001. Phase relations of peralkaline silicic magmas and petrogenetic implications. J. Petrol. 42, 825–845. doi:10.1093/petrology/42.4.825

Sharp, Z., 1990. A laser-based microanalytical method for the in situ determination of oxygen isotope ratios of silicates and oxides. Geochim. Cosmochim. Acta 54, 1353–1357. doi:10.1016/0016-7037(90)90160-M

Teklay, M., Kröner, A., Mezger, K., Oberhänsli, R., 1998. Geochemistry, Pb-Pb single zircon ages and Nd-Sr isotope composition of Precambrian rocks from southern and eastern Ethiopia: implications for crustal evolution in East Africa. J. African Earth Sci. 26, 207–227. doi:10.1016/S0899-5362(98)00006-2

Teklemariam, M., Battaglia, S., Gianelli, G., Ruggieri, G., 1996. Hydrothermal alteration in the Aluto-Langano geothermal field, Ethiopia. Geothermics 25, 679–702. doi:10.1016/S0375-6505(96)00019-3

Watson, E.B., 1979. Zircon saturation in felsic liquids: Experimental results and applications to trace element geochemistry. Contrib. to Mineral. Petrol. 419, 407–419.

White, J.C., Parker, D.F., Ren, M., 2009. The origin of trachyte and pantellerite from Pantelleria, Italy: Insights from major element, trace element, and thermodynamic modelling. J. Volcanol. Geotherm. Res. 179, 33–55. doi:10.1016/j.jvolgeores.2008.10.007

Wolfenden, E., Ebinger, C., Yirgu, G., Deino, A., Ayalew, D., 2004. Evolution of the northern Main Ethiopian rift: birth of a triple junction. Earth Planet. Sci. Lett. 224, 213–228. doi:10.1016/j.epsl.2004.04.022

Wolfenden, E., Ebinger, C., Yirgu, G., Renne, P.R., Kelley, S.P., 2005. Evolution of a volcanic rifted margin: Southern Red Sea, Ethiopia. Geol. Soc. Am. Bull. 117, 846. doi:10.1130/B25516.1

Xu, W., Rivalta, E., Li, X., 2017. Magmatic architecture within a rift segment: Articulate axial magma storage at Erta Ale volcano, Ethiopia. Earth Planet. Sci. Lett. 476, 79–86. doi:10.1016/j.epsl.2017.07.051

Figure Captions

Figure 1. Topographic maps summarizing geotectonic setting and crustal structure in Ethiopia. In (**a**) the black lines represent major plate boundaries, coloured symbols identify the volcanic systems considered in this study, and the grey square corresponds to the inset b. The major terrestrial rift zones are: the Afar Rift (AR); the Main Ethiopian Rift (MER) and Kenyan Rift (KR). Within each rift volcanic activity is localized in magmatic segments. Dabbahu and Badi are located on and off the Manda Hararo Rift Segment (MHRS) of the Afar Rift (inset b), while the Erta Ale range lies in the Erta Ale Segment (EAS). Aluto, Gedemsa and Kone are located along the MER, but Kone lies in a different magmatic segment from Aluto and Gedemsa. White arrows show current extension vectors relative to a fixed Nubian Plate (after Saria et al., 2014). (**b**) Hillshade digital elevation model of the MHRS showing the location of Dabbahu and Badi silicic volcanic systems. The black dashed line identifies the rift axis and the orange area represents the focus of recent dyke intrusion, faulting and eruptions (Ferguson et al., 2010). **(c)** A summary of crustal sections adjacent to the volcanic systems considered in this study. Sections are based on controlled source seismic experiments and receiver function studies (after Hammond et al., 2011 and references therein). Section locations are shown as circled numbers on the topographic map (a). Approximate depths of silicic magma reservoirs are based on

deformation (Hutchison et al., 2016c), seismic and petrological constraints (Field et al., 2012a; Gleeson et al., 2017).

Figure 2. Selected major element classification diagrams (all data are anhydrous normalized). (**a**) Total alkalis versus silica (TAS) diagram. The grey dashed line shows the alkaline sub-alkaline (tholeiitic) divide of Irvine and Baragar (1971). Rhyolites with low alkalis (<8 wt. %) often have anomalous low Na_2O and high loss on ignition values suggestive of post-emplacement alteration (Peccerillo et al., 2003). (**b**) Peralkalinity index (PI) versus Aluminium Saturation Index (ASI) is used to define metaluminous, peraluminous and peralkaline composition fields for silicic rocks. PI is defined as the molar $(Na_2O+K_2O) / Al_2O_3$ while ASI is defined as the molar ratio $Al_2O_3 / (CaO + K_2O + Na_2O)$. For each volcanic system the most peralkaline samples are labelled. (**c**) Peralkaline classification diagram (Al_2O_3 versus FeO_t) based on Macdonald (1974).

Figure 3. Major element Harker diagrams of whole-rock compositions determined by XRF. Best-fit Rhyolite-MELTS liquid lines of descent for Aluto and Dabbahu are overlain (black dashed lines). The model parameters are provided in Table 3. Inaccuracies in apatite crystallization for peralkaline systems in Rhyolite-MELTS explain the poor fit between the data and models for P_2O_5. A schematic showing a more likely liquid line of descent for P_2O_5 is provided and illustrates how mixed samples fall beneath the peak. Natural samples that show textural evidence for magma mixing are circled by the grey dashed line.

Figure 4. Selected trace element compositions for the volcanic systems. The influence of magmatic differentiation and certain fractionating mineral phases are shown by the black arrows. Data for ~30 Ma comendite ignimbrites associated with flood basalt volcanism (after, Ayalew et

al., 2002 and Ayalew and Yirgu, 2003) are shown as dark grey shaded fields (with asterisk in bottom right hand plot). Pan-African Precambrian crust trace element data are from Peccerillo et al. (1998).

Figure 5. Isotopic constraints on magma petrogenesis. **a)** $\delta^{18}O_{melt}$ evolution predicted by model fractional crystallization (FC) scenarios compared to data from across Ethiopia. For clarity samples are arranged according to their rock type (total alkalis-silica classification) so that fractionation increases from left to right. Data point colours relate to each volcanic system; symbol style corresponds to the material analysed. To correct $\delta^{18}O_{mineral}$ to $\delta^{18}O_{melt}$ we used experimentally determined fraction factors of Appora et al. (2003). The $\delta^{18}O_{melt}$ trajectory for our best-fit Rhyolite-MELTS models is shown by the grey shaded region (labelled FC trajectory). Fractional crystallization scenarios predict a moderate increase in $\delta^{18}O_{melt}$ assuming a parental melt range of 5.0–5.8 ‰ (see text for detailed discussion). Samples that fall off the FC trajectory have been contaminated by Pan-African Precambrian crustal rocks (high $\delta^{18}O$) or hydrothermally altered crust (low $\delta^{18}O$), which we have assigned end-member values of 12 ‰ and 2 ‰ respectively (Section 5.1). Orange and blue lines above and below the FC trajectory provide estimates for the amount of end-member crustal melt that would need to be assimilated in order to explain $\delta^{18}O_{melt}$. New $\delta^{18}O$ are presented in Table 2. Erta Ale and MHRS $\delta^{18}O$ are from Barrat et al. (1998, 2003). ~30 Ma ignimbrites are from Ayalew et al. (2002). **b)** ε_{Nd} and $^{87}Sr/^{86}Sr$ constraints on crustal assimilation in Ethiopia. Symbol colours are the same as a), while symbol style corresponds to rock type. All isotopes for ~30 Ma samples are age-corrected (see Rooney, 2017, and references therein). New analyses are from Dabbahu, Badi and MHRS while previous analyses are compiled from: Barrat et al. (1998, 2003); Peccerillo et al., (2003, 2007); Furman et al. (2006); Giordano et al. (2014) and Ayalew et al., (2016). The field of MER and Afar Rift

Quaternary basalts (assumed representative of Ethiopian mantle) are outlined by the black dotted line (see Ayalew et al., 2016 and references therein). A Pan-African lithosphere endmember (after Rooney et al., 2012c) is shown by the grey star while a typical uncontaminated mantle-derived melt from Afar is shown by the white star. Binary mixing models for pristine mantle-derived pantellerite and basalt compositions with Pan-African crust are shown by the black lines at increments of 5 %. Mixing of partial melts of granitoid rocks (equivalent to Pan-African crustal materials using batch melting models) with uncontaminated-endmembers produced similar trends to those shown and for figure clarity these are not displayed. The end-members used in the model had Sr and Nd concentrations as follows: pantellerite: 5 and 200 ppm; basalt: 500 and 30 ppm and Pan-African: 225 and 22 ppm (in accordance with Rooney et al., 2012c).

Figure 6. Comparison of erupted volumes, fluxes and melt evolution for the volcanic systems and a summary of key findings. **a)** The total erupted volume of each volcanic system (Table 4) is shown by the upper coloured bars and is plotted against local crustal thickness (after Hammond et al., 2011). Cumulate volumes are shown by the lower, darker bars and were calculated using Rhyolite-MELTS models (see text). **b)** Eruptive and cumulate fluxes are shown for each system and were calculated using available age constraints (Tables 1, 4). Two flux bars are shown for Dabbahu, using two estimates for the age of the system (300 and 500 ka, Tables 1, 4). **c)** The average Zr content of the most evolved samples for each volcanic system plotted against the erupted volume flux (b). Each system is represented by a different coloured symbol. To get a representative sample of the most evolved components of each volcanic system we average the Zr concentration of the silicic samples with highest Zr (which we define as the upper quartile of the data). There is a clear negative relationship between eruptive flux and average Zr (i.e. melt evolution). This suggests that local magma supply is an important control on fractional

crystallization and melt evolution processes. **d)** Schematic summarizing crustal structures of the EAS, MHRS and MER and petrological constraints on magmagenesis. Grey colours represent intrusive melts while orange rectangles represent cumulate bodies. Blue spirals reflect hydrothermal circulation that generates low $\delta^{18}O$ crust. Abbreviations: RF: rift fill (i.e., lavas and sedimentary cover); UC: upper crust; LC: lower crust. Intermediate-mature continental rift zones (e.g., MER and MHRS) promote extreme melt evolution since parental basalts are transitional in composition and local magmatic flux is low.

Table 1. Summary of the geological setting, eruptive history and age constraints for the six volcanic systems considered in this study. Note the following abbreviations: MER: Main Ethiopian Rift; AG: Aluto-Gedemsa; BK: Boseti-Kone; MHRS: Manda Hararo Rift Segment and EAS: Erta Ale Segment.

rift zone	volcanic system (magmatic segment)	eruptive history/setting	age constraints	key references
MER	Aluto (AG segment)	Initially built up as a trachytic complex before undergoing caldera collapse. Significant volumes of post-caldera silicic volcanism then took place rebuilding the main edifice.	Caldera forming eruption took place at 316 ± 19 ka and 306 ± 12 ka; post-caldera volcanism initiated at 55 ±19 ka with recent eruptions in last 1 ka	Hutchison et al., 2016a, b; Gleeson et al., 2017
	Gedemsa (AG segment)	Initial activity built up a trachytic-rhyolitic complex. Caldera collapse then took place possibly via multiple explosive eruptions. Finally, a set of small coalescing post-caldera silicic edifices and fissure basalts were erupted in the centre of the caldera.	K/Ar dating places pre-caldera samples 320 ± 20 ka and post-caldera samples 260 ± 20 ka	Peccerillo et al., 2003; Giordano et al., 2014
	Kone (BK segment)	Pre-caldera activity built up a trachytic cone. Then four major eruptive phases took place and generated a large collapse scar. Post-caldera mafic eruptions have partially infilled the collapse and very minor silicic eruptions have occurred around the ring fracture.	None	Rampey et al. 2010, 2014
Afar Rift	Badi (MHRS)	Badi is an off-axis silicic volcano (Figure 1b) - it is composed of coalescing lava flows and domes and no caldera collapse scars are observed.	Earliest eruptions dated at 290 ± 4 ka (K/Ar age for a rhyolitic flow near base of edifice), recent basaltic lavas dated between ~140 and 25 ka	Lahitte et al., 2003; Ferguson et al., 2013b
	Dabbahu (MHRS)	Dabbahu is an on-axis volcano (Figure 1b). The central edifice comprises coalescing flows and domes that span an almost complete basalt–peralkaline rhyolite compositional series. No large-volume ignimbrite deposits or caldera features have yet been identified.	$^{40}Ar/^{39}Ar$ indicate multiple eruptive cycles between 60 and 5 ka, cosmogenic ^{3}He ages suggest Dabbahu has been active for >100 ka	Barberi et al., 1975; Field et al., 2012a,2013; Medynski et al., 2013
	Erta Ale (EAS)	The ~80 km Erta Ale range forms an axial volcanic ridge comprising six distinct eruptive centres (Gada Ale, Alu-Dalafilla, Borale Ale, Erta Ale, Hayli Gubbi and Ale Bagu). Magma compositions range from transitional alkali-tholeiitic basalt to rhyolite.	Age constraints on onset of volcanism are limited, oldest K/Ar are ~1000 ka	Barberi and Varet, 1970; Barberi et al., 1972; Bizourd et al., 1980; Barrat et al., 1998; Beyene and Abdelsalam, 2005

Table 2. New oxygen isotope data for Ethiopian volcanic systems.

volcanic system[a]	**sample code**	**rock type**[b]	**material analysed**	**$\delta^{18}O$ (‰ V-SMOW)**	**age (stratigraphic context)**[c]
Aluto	15-02-09	trachyte	glass	6.5	570–330 ka (pre-caldera)[1]
	01-02-14	pantellerite	glass	6.2	62 ± 13 ka (post-caldera)[1]
	18-02-04	comendite	glass	6.1	55 ± 19 ka (post-caldera)[1]
	02-02-12	pantellerite	glass	6.2	60–10 ka (post-caldera)[1]
	31-01-LE	pantellerite	glass	6.4	16 ± 14 ka (post-caldera)[1]
	15-01-07B	TA	glass	5.2	n.d. (post-caldera)[1]
	18-11-01	BTA	glass	6.0	n.d. (post-caldera)[1]
	01-02-13	pantellerite	glass	6.2	<10 ka (post-caldera)[1]
Gedemsa[d]	GD22	rhyolite	alkali feldspar	7.9	>300 ka (pre-caldera)[2]
	GD3	basalt	olivine	5.8	<300 ka (post-caldera)[2]
	GD8	pantellerite	alkali feldspar	6.2	<300 ka (post-caldera)[2]
	GD12	pantellerite	alkali feldspar	7.3	<300 ka (post-caldera)[2]
	GD15	salic xenolith	alkali feldspar	6.8	n.d. (enclave in post-caldera rocks)[2]
Kone	2-11	rhyolite	glass	7.1	n.d. (pre-caldera)[3]
	3-30	pantellerite	glass	5.9	n.d. (post-caldera)[3]
	4-11	pantellerite	glass	6.2	n.d. (post-caldera)[3]
	3-34	pantellerite	glass	6.1	n.d. (post-caldera)[3]
	4-21	basalt	glass	5.2	n.d. (post-caldera)[3]
	2-20	basalt	glass	5.5	n.d. (post-caldera)[3]
	3-31	basalt	glass	5.6	n.d. (post-caldera)[3]
	2-22	basalt	glass	5.4	n.d. (post-caldera)[3]
Badi	3016	basalt	glass	6.1	n.d. [4]
	29 09	TA	glass	6.0	138.9 ± 1.1 ka [4]
	29 11	basalt	glass	5.3	54.5 ± 5.6 ka [4]
	Bad 4	basalt	olivine	4.8	39.8 ± 3.7 ka [5]
	Bad 5	basalt	olivine	5.0	39.8 ± 3.7 ka [5]
	BADI 05	basalt	glass	5.1	25.4 ± 9.4 ka [4]
	24 02	pantellerite	glass	5.6	n.d. [4]
	30 12	pantellerite	glass	6.0	n.d. [4]
	03 04	pantellerite	glass	6.5	n.d. [4]
	BADI 07	pantellerite	glass	6.2	n.d. [4]
MHRS axis	Dik 2	basalt	olivine	5.2	68.2 ± 3.3 ka [5]
	Dik 3	basalt	olivine	5.2	68.2 ± 3.3 ka [5]
	Gab I	basalt	olivine	5.1	66.1 ± 5.4 ka [5]
	Gab G3	basalt	olivine	5.2	<2 ka [5]
	2007	basalt	glass	5.3	2007 (fissure eruption)[6]
	Gab B	basalt	olivine	5.3	n.d. [5]
Dabbahu	LFAF 044	basalt	glass	5.4	>60 ka [7]
	LFAF 045	basalt	glass	4.9	>60 ka [7]
	LFAF 028	TB	glass	5.3	63–48 ka [7]
	LFAF 106	TA	glass	6.4	63–48 ka [7]
	LFAF 047a	BTA	glass	6.0	~49 ka [7]
	LFAF 054	commendite	glass	5.7	30.1 ± 0.4 ka [7]
	LFAF 011	comendite	glass	7.8	28.6 ± 0.7 ka [7]
	LFAF 055	pantellerite	glass	5.7	<10 ka [7]
	LFAF 063	pantellerite	glass	5.5	<10 ka [7]

[a] Erta Ale $\delta^{18}O$ data (not shown) was presented in Barrat et al. (1998)

[b] Rock type abbreviations include: TB: trachybasalt; BTA: basaltic trachyandesite and TA: trachyandesite.

[c] Age and stratigraphic constraints are provided (when available) in the right-hand column. n.d. indicates that no age data is currently available. Superscripts refer to prior published samples: 1: Hutchison et al. (2016a, b); 2: Peccerillo et al. (2003); 3: Rampey (2005); 4: Ferguson et al. (2013b); 5: Medynski et al. (2013); 6: Ferguson et al. (2010) and 7: Field et al. (2013).

[d] Gedemsa $\delta^{18}O$ data were generated by Peccerillo et al. (2003). Note that sample labels for $\delta^{18}O$ have been updated here following discussion with the authors (Peccerillo pers. comm.).

Table 3. Best-fit magma storage conditions for Aluto and Dabbahu constrained via Rhyolite-MELTS models and the range of input parameters that were explored. Note that we use a minimization routine developed by Gleeson et al. (2017) to identify the model storage conditions that most closely match the whole-rock compositions of the pantellerites (i.e., the most chemically-evolved samples).

		Aluto	Dabbahu
parameter range explored	pressure (MPa)	50–300	50–400
	H_2O content (wt. %)	0.5–3	0.5–2
	fo_2 (log units relative to QFM)	−2 to +1	0 to −1
Rhyolite-MELTS best-fit	pressure (MPa)	150	150
	H_2O content (wt. %)	0.5	0.5
	fo_2 (log units relative to QFM)	0	0
	starting composition	primitive rift-related basalt (17-01-05) sampled north-east of the complex	high MgO (>8 wt. %) basaltic sample LFAF 044 (Field et al., 2013)
	bulk density of crystal cumulate (kg m^{-3})	3060	3040
petrological constraints		granophyric textures in some rhyolitic samples indicate crystallisation at shallow depths (~100 MPa)	melt inclusions suggest shallow storage <250 MPa. Fe-Ti oxides constrain fO_2 between QFM and QFM-1. 4±1 wt. % H_2O in rhyolites suggests ~0.5% H_2O in parent
relevant studies		Hutchison et al., 2016; Gleeson et al., 2017	Field et al., 2012a, 2013

Table 4. Erupted and cumulate volume estimates for the volcanic systems considered in this study.

volcanic system (eruption onset estimate)[a]	erupted volumes (from DEM)[b]			cumulate volumes (from Rhyolite-MELTS)[c]		cumulate volume: erupted volume	local rift volume filled by cumulate (%)[d]
	deposit volume (km^3)		eruptive flux (km^3 ka^{-1})	cumulate volume (km^3)	cumulate flux (km^3 ka^{-1})		
Aluto (500 ka)	pre-caldera edifice	48		145			
	caldera collapse	20		60			
	post-caldera	32		98			
	total	99	0.20	302	0.60	3.0	23
Gedemsa (500 ka)	pre-caldera edifice	33		135			
	caldera collapse	30		122			
	post-caldera	1		6			
	total	64	0.13	263	0.53	4.1	30
Kone (500 ka)	pre-caldera edifice	10		54			
	caldera collapse	15		75			
	total	25	0.05	129	0.26	5.2	25
Badi (300 ka)	edifice	29	0.10	92	0.31	3.2	9
Dabbahu (500–300 ka)	edifice	114	0.23–0.38	454	0.91–1.51	4.0	16–27
Erta Ale (1000 ka)	magmatic segment	405	0.41	209	0.21	0.5	1

[a] The timing of eruption onsets at each system are not known precisely; we used best-estimates from existing geochronologies (Table 1). For the MER volcanoes, age constraints suggest initial eruptions at ~500 ka (i.e, between 750 and 300 ka, Hutchison et al., 2016a). At Badi we use a K/Ar age of ~300 ka from the base as the eruption onset (Lahitte et al., 2003). At Dabbahu, the oldest deposits are poorly exposed and although cosmogenic ^{3}He ages (Medynski et al., 2013) indicate ages >100 ka no precise age is known for eruption onset. Instead we evaluate a range of values between 300 ka (assuming Dabbahu is equivalent in age to neighbouring Badi) and 500 ka (i.e. the minimum age of basalts on external margins of the MHRS which Dabbahu overlaps, Lahitte et al., 2003). The onset of volcanism in the Erta Ale magmatic segment is generally placed at less than ~1000 ka (see review of Beyene and Abdelsalam, 2005, based on K/Ar dating from Barberi et al., 1972).

[b] Erupted volumes are calculated from digital elevation models (DEMs) following methods outlined by Hutchison et al., (2016a). At Aluto and Gedemsa it is possible to identify pre-, syn- and post-caldera phases. At Kone, post-caldera deposits are widely distributed but very minor in areal extent and have not been included in the long-term eruptive volume budget. At Badi and Dabbahu, caldera collapse phases are poorly

documented so we calculate the volume of the edifice. At Erta Ale, we calculated the volume of the entire magmatic segment, which includes six volcanic centres: Gada Ale, Alu-Dalafilla, Borale Ale, Erta Ale, Hayli Gubbi and Ale Bagu. We estimate cumulate volumes from whole rock Zr data, and Rhyolite-MELTS models (details in Section 5.4).

[c] Cumulate fluxes and volumes are minima because they are based on erupted volumes and exclude any evolved magmas that did not erupt.

[d] Percentage of rift volume (created by extension) that would be filled by magmatic cumulate. To estimate the volume created by extension at each volcanic system we use the local crustal thickness (Figure 6a), extension rate (Figure 2) and their along-axis length (measured from DEMs).

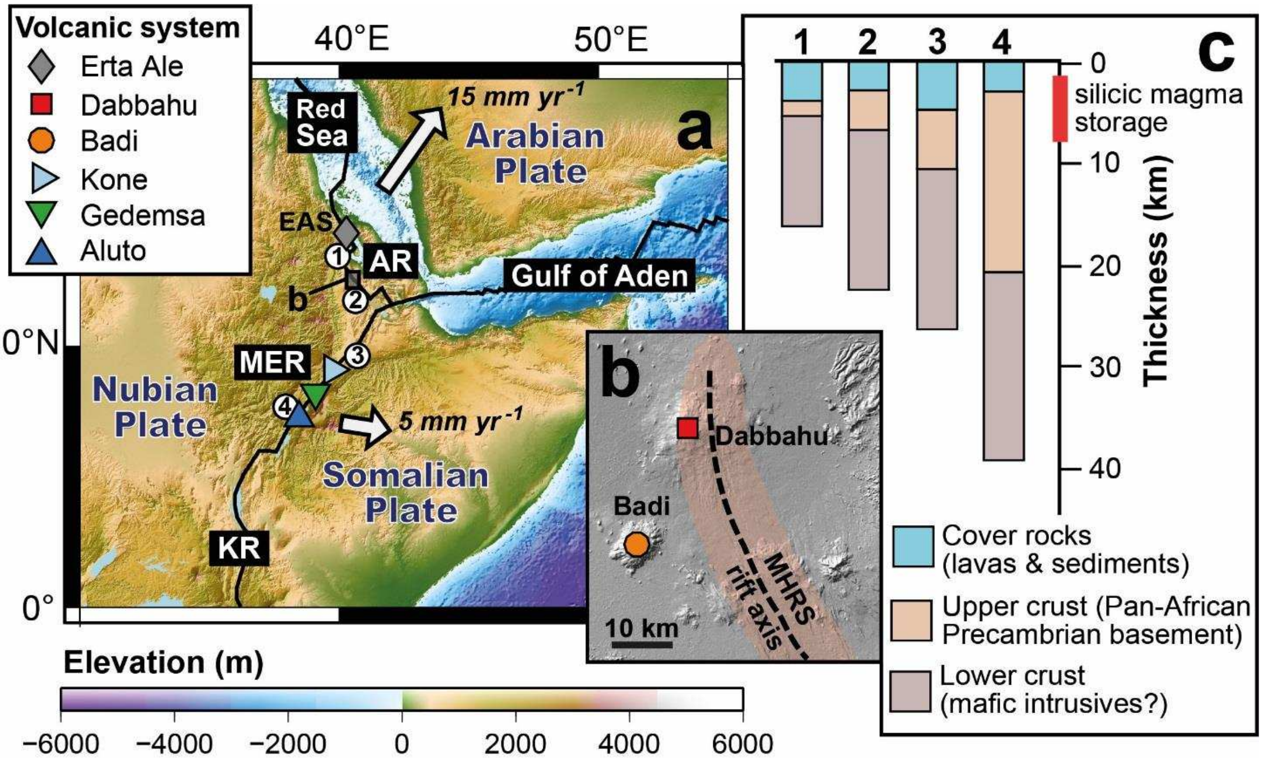

Volcanic system
Erta Ale
Dabbahu
Badi
Kone
Gedemsa
Aluto
40°E
50°E
10°N
0°
a
Red Sea
15 mm yr-1
Arabian Plate
EAS
AR
Gulf of Aden
b
MER
Nubian Plate
5 mm yr-1
Somalian Plate
KR
Elevation (m)
−6000
−4000
−2000
0
2000
4000
6000
b
Dabbahu
Badi
MHRS rift axis
10 km
c
1
2
3
4
silicic magma storage
Thickness (km)
0
10
20
30
40
Cover rocks (lavas & sediments)
Upper crust (Pan-African Precambrian basement)
Lower crust (mafic intrusives?)

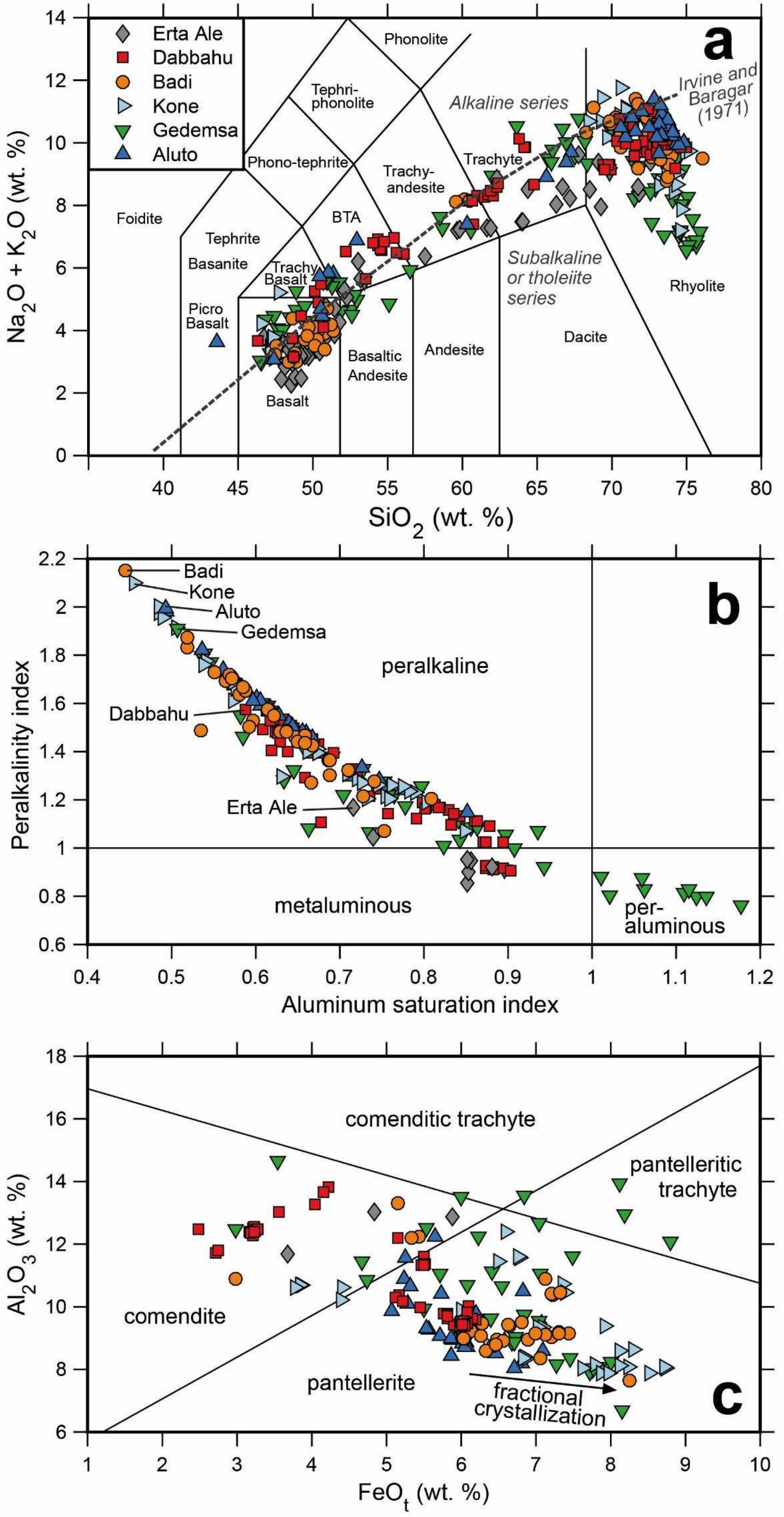

a
Erta Ale
Dabbahu
Badi
Kone
Gedemsa
Aluto
Phonolite
Tephri-phonolite
Phono-tephrite
Trachy-andesite
Trachyte
Alkaline series
Irvine and Baragar (1971)
Foidite
Tephrite
Basanite
BTA
Trachy Basalt
Picro Basalt
Basalt
Basaltic Andesite
Andesite
Dacite
Subalkaline or tholeiite series
Rhyolite
$Na_2O + K_2O$ (wt. %)
SiO_2 (wt. %)
b
Badi
Kone
Aluto
Gedemsa
Dabbahu
Erta Ale
peralkaline
metaluminous
per-aluminous
Peralkalinity index
Aluminum saturation index
c
comenditic trachyte
pantelleritic trachyte
comendite
pantellerite
fractional crystallization
Al_2O_3 (wt. %)
FeO_t (wt. %)

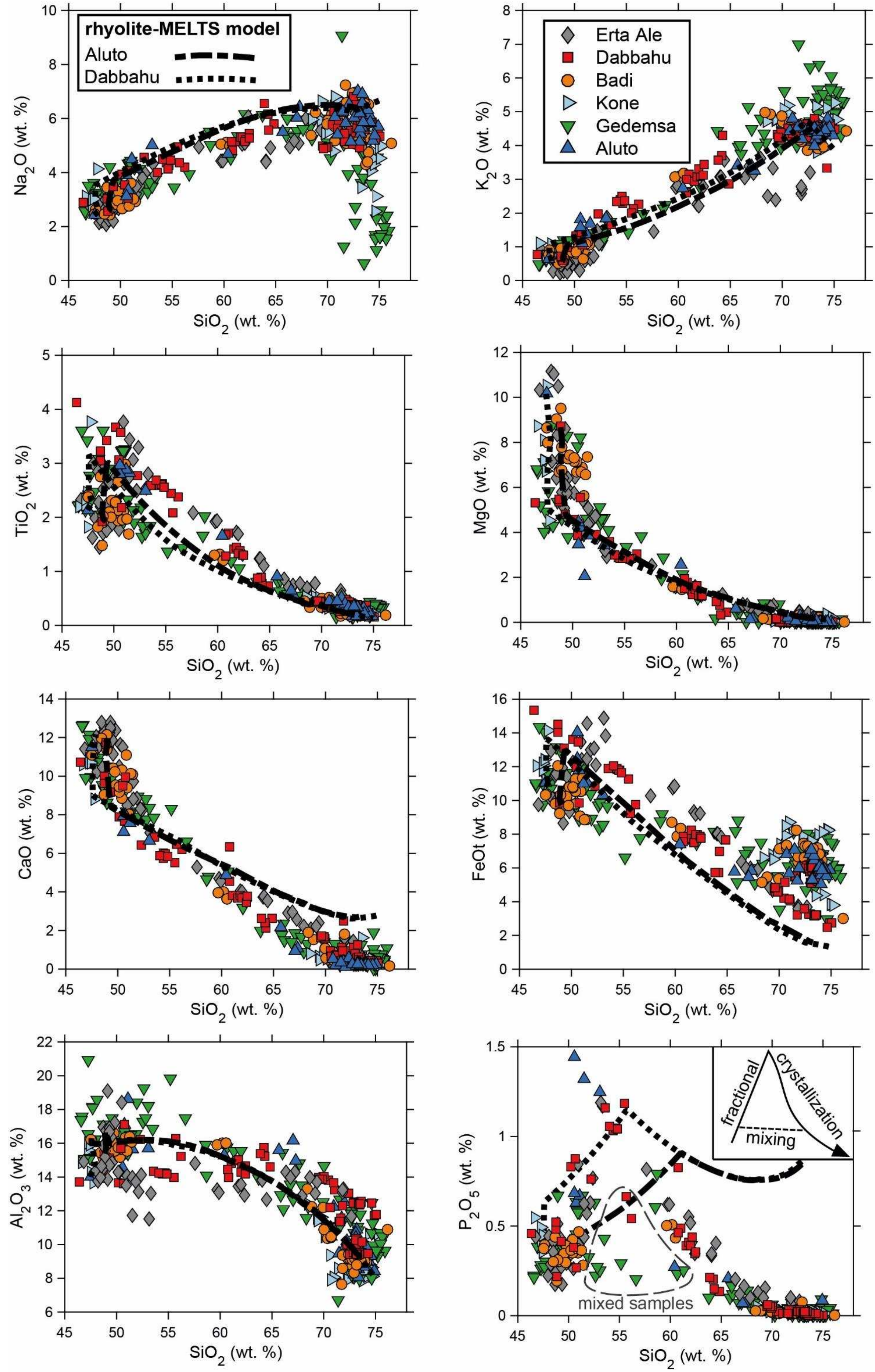
rhyolite-MELTS model
Aluto
Dabbahu
Erta Ale
Dabbahu
Badi
Kone
Gedemsa
Aluto
Na_2O (wt. %)
K_2O (wt. %)
TiO_2 (wt. %)
MgO (wt. %)
CaO (wt. %)
FeOt (wt. %)
Al_2O_3 (wt. %)
P_2O_5 (wt. %)
SiO_2 (wt. %)
fractional
crystallization
mixing
mixed samples

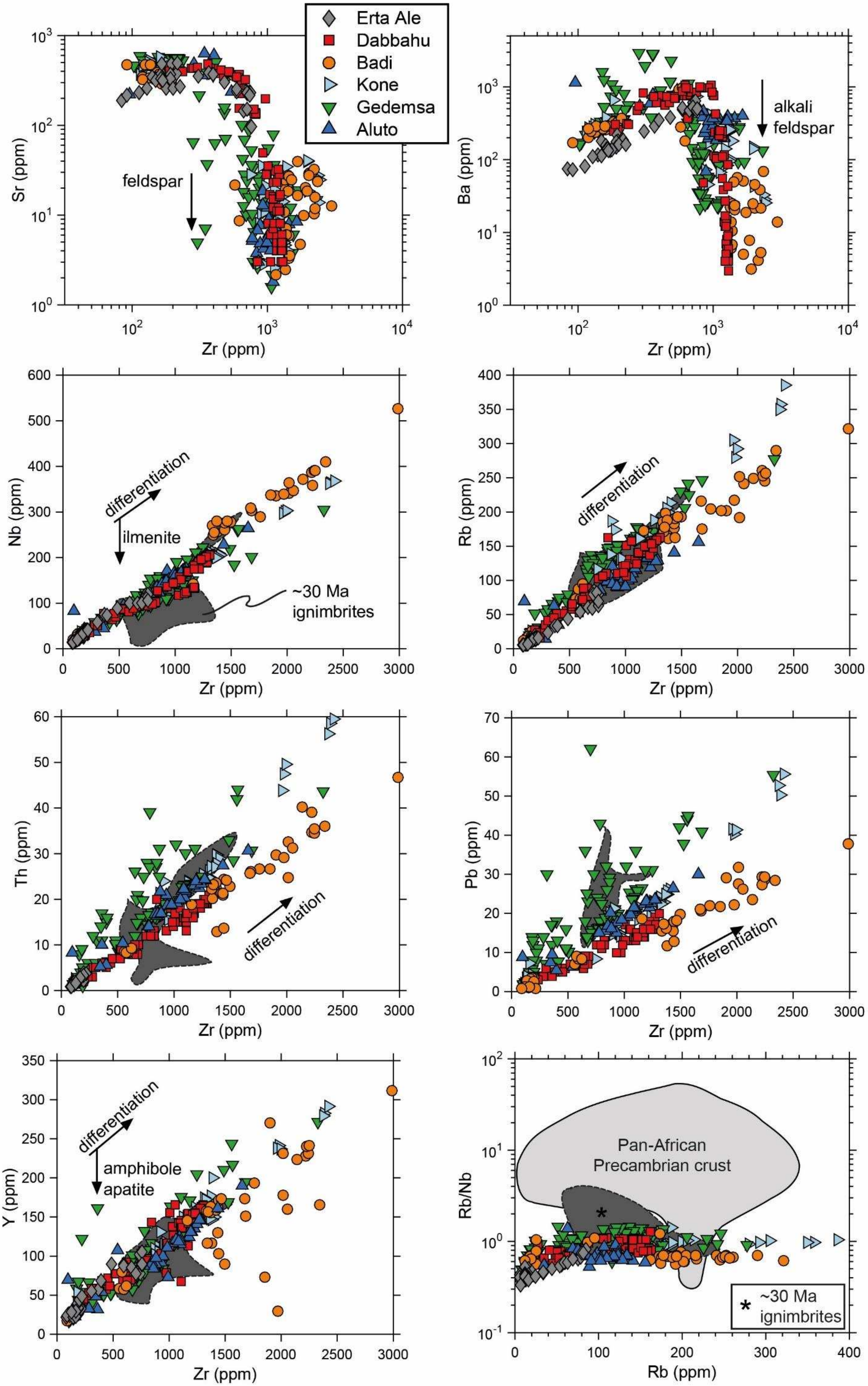
Erta Ale
Dabbahu
Badi
Kone
Gedemsa
Aluto
Sr (ppm)
Zr (ppm)
feldspar
Ba (ppm)
alkali feldspar
Nb (ppm)
differentiation
ilmenite
~30 Ma ignimbrites
Rb (ppm)
Th (ppm)
Pb (ppm)
Y (ppm)
amphibole apatite
Rb/Nb
Rb (ppm)
Pan-African Precambrian crust
* ~30 Ma ignimbrites

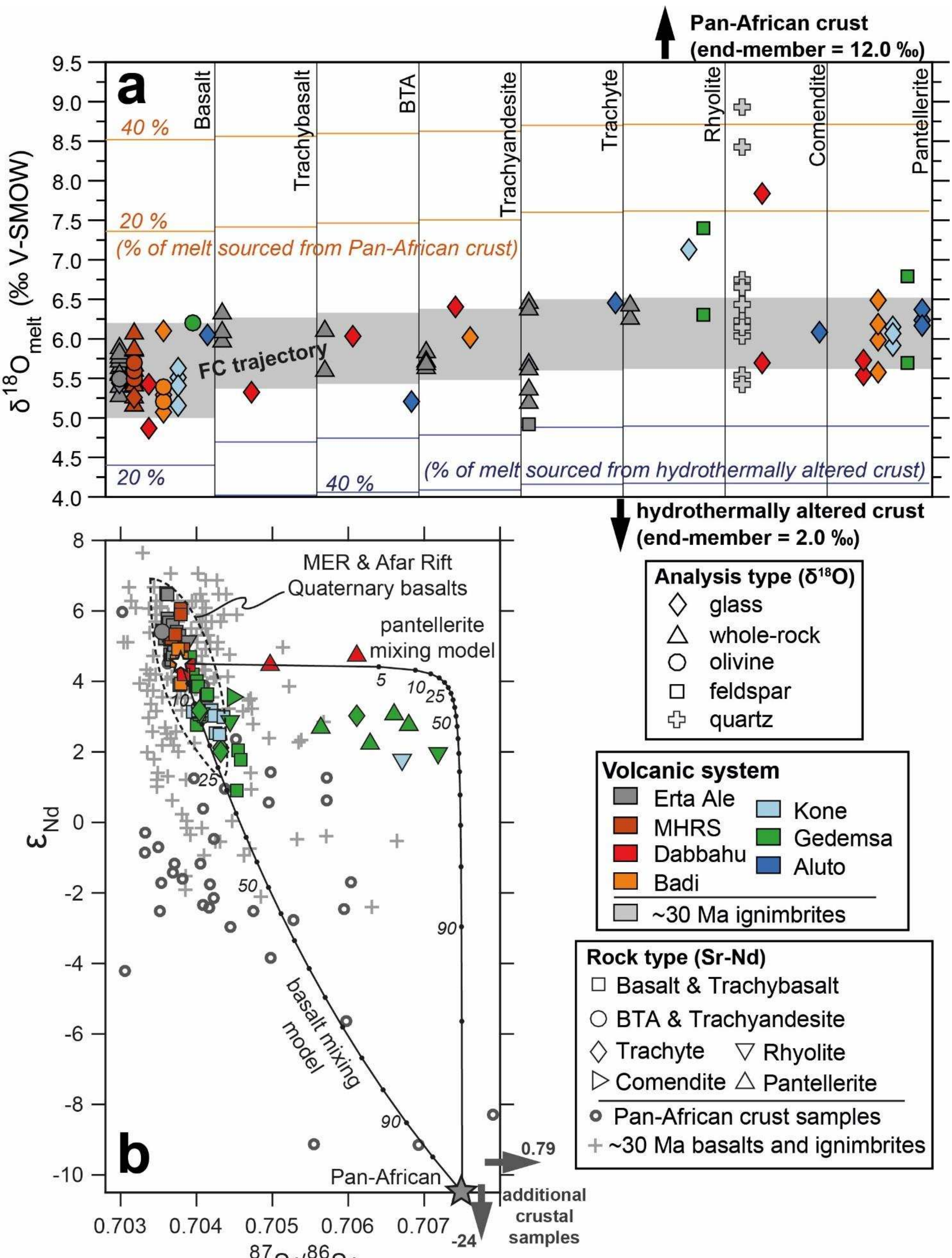

Pan-African crust
(end-member = 12.0 ‰)
a
Basalt
Trachybasalt
BTA
Trachyandesite
Trachyte
Rhyolite
Comendite
Pantellerite
40 %
20 %
(% of melt sourced from Pan-African crust)
FC trajectory
20 %
40 %
(% of melt sourced from hydrothermally altered crust)
δ18Omelt (‰ V-SMOW)
hydrothermally altered crust
(end-member = 2.0 ‰)
MER & Afar Rift
Quaternary basalts
pantellerite
mixing model
basalt mixing
model
Pan-African
b
0.79
additional
crustal
samples
-24
εNd
87Sr/86Sr
Analysis type (δ18O)
glass
whole-rock
olivine
feldspar
quartz
Volcanic system
Erta Ale
MHRS
Dabbahu
Badi
Kone
Gedemsa
Aluto
~30 Ma ignimbrites
Rock type (Sr-Nd)
Basalt & Trachybasalt
BTA & Trachyandesite
Trachyte
Rhyolite
Comendite
Pantellerite
Pan-African crust samples
~30 Ma basalts and ignimbrites

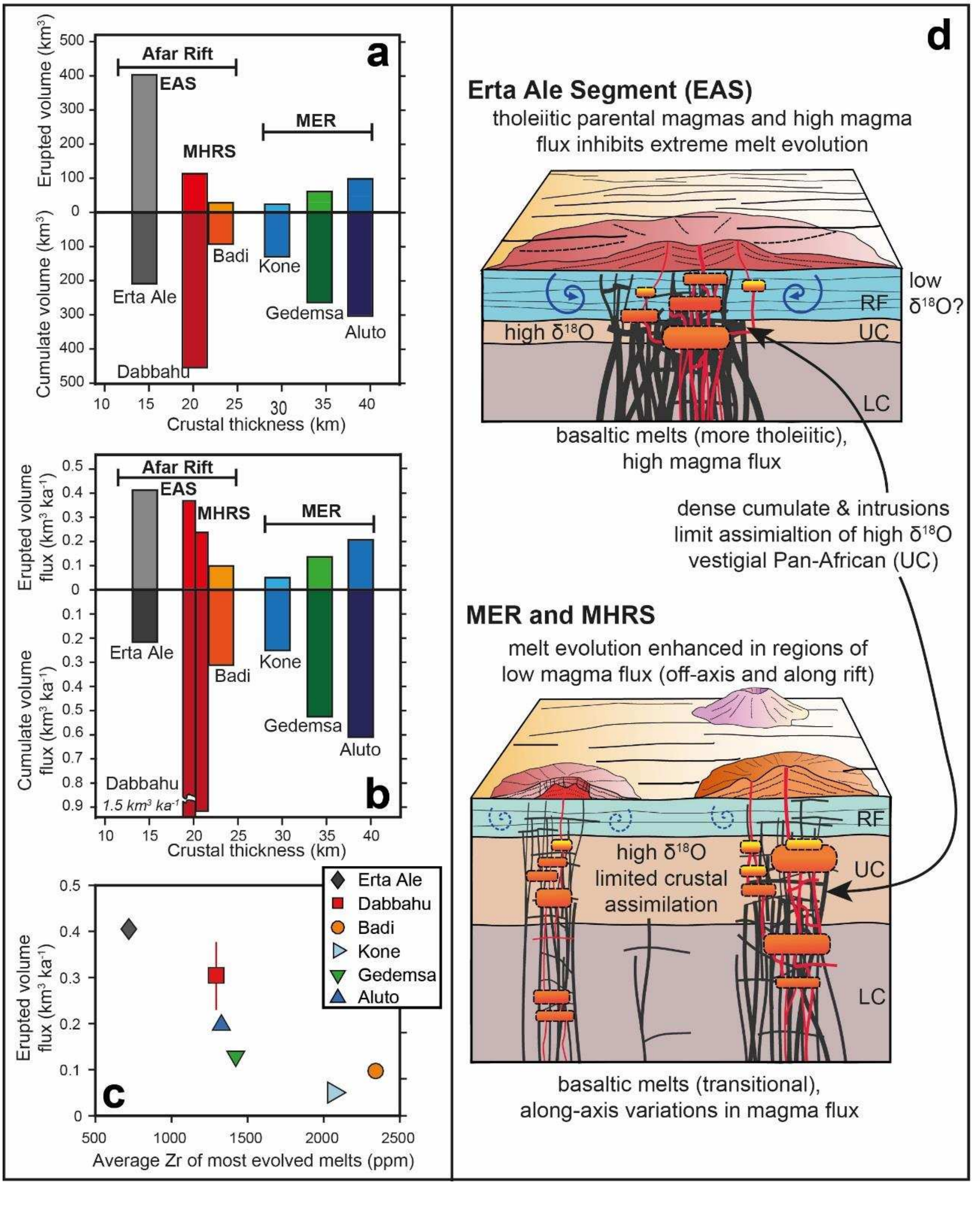

a
Afar Rift
EAS
MHRS
MER
Erupted volume (km³)
Cumulate volume (km³)
Erta Ale
Dabbahu
Badi
Kone
Gedemsa
Aluto
Crustal thickness (km)
b
Erupted volume flux (km³ ka⁻¹)
Cumulate volume flux (km³ ka⁻¹)
1.5 km³ ka⁻¹
c
Erupted volume flux (km³ ka⁻¹)
Average Zr of most evolved melts (ppm)
d
Erta Ale Segment (EAS)
tholeiitic parental magmas and high magma flux inhibits extreme melt evolution
low δ¹⁸O?
RF
UC
LC
high δ¹⁸O
basaltic melts (more tholeiitic), high magma flux
dense cumulate & intrusions limit assimialtion of high δ¹⁸O vestigial Pan-African (UC)
MER and MHRS
melt evolution enhanced in regions of low magma flux (off-axis and along rift)
high δ¹⁸O limited crustal assimilation
basaltic melts (transitional), along-axis variations in magma flux